Novel object-place configurations increase excitability of layer 5 lateral entorhinal cortex engram cells

Banks PJ[1,2,*] & Barker GRI[1,2], Booth CA[1], Kinnavane L[1], Warburton EC[1,3] & Bashir ZI[1,3,*]

[1]School of Physiology, Pharmacology and Neuroscience, University of Bristol, Biomedical Sciences Building, University Walk, Bristol BS8 1TD, United Kingdom

[2,3]These authors contributed equally to the study

*Correspondence: paul.banks@bristol.ac.uk; z.i.bashir@bristol.ac.uk

Abstract

Associative recognition memory is essential for our everyday lives, allowing us to form cognitive representations of and remember relationships between things we encounter and their environments, such as where we left our keys or parked the car. Evidence suggests that these associations are represented in the lateral entorhinal and medial prefrontal cortices. However, the identity of neurons in which these associations are formed, the cellular mechanisms supporting them and how representations of object-associations react to changes in the environment are not understood. Here we use transgenic mice to label associative recognition memory engrams in mice, finding that memory recall reactivates engram cells in multiple cortical regions, but that engram cell reactivation only correlates with behavioural performance in the dorsolateral entorhinal cortex, where reactivation was highest in layer 5/6. Chemogenetic inhibition of engram cells in lateral entorhinal cortex impaired memory retrieval. Electrophysiology from e*x vivo* slices following memory recall demonstrated that engram cells in lateral entorhinal cortex layer 5, but not other cortices or layers, showed increased excitability only when the engram-specific objects had been reconfigured. These data collectively identify neurons in deep layers of lateral entorhinal cortex as probable loci of object-place associations and propose a mechanism by which new information is incorporated into pre-existing neural representations.

Introduction

Associative recognition memory, remembrance for objects and their associated locations and contexts, is fundamental to everyday decision making and behaviour. These memories depend on a highly interconnected brain network including the hippocampus, thalamus, perirhinal cortex (PRH), medial prefrontal cortex (mPFC) and the medial and lateral entorhinal cortex (LEC)[1]. Of these cortical regions, PRH has a well-established role encoding object identity and novelty, whilst mPFC performs integration of object identity, location and time[2,3]. The role of LEC, however, is less clear.

Classical models[4] propose that LEC is part of a processing stream representing object features and identity, which converges with spatial information to form object-context representations in the hippocampus. Emerging evidence however suggests that LEC neurons can represent dimensions not only of object identity but also of context, time and space[5-12]. Indeed, lesion or inactivation of LEC impairs object-in-place (OiP) and object-in-context (OiC) memory whilst sparing simple novel object recognition[13-16] (though see[17]).

Which neurons in these association cortices are prominently active during OiP memory and the plastic changes which may support memory is unclear; both superficial and deep LEC neurons have been shown to encode multi-dimensional object representations[7,8,12]. Optogenetic inhibition[16] of mPFC→LEC synapses, which innervate deep layers of LEC[16,18], impairs both OiP and OiC memory whilst LEC layer 2a fan cells are crucial for associative learning[19] and object-context-place discrimination[17]. For mPFC, immediate-early gene studies have shown activation of mPFC by associative recognition memory tasks, but have not examined laminar activation in detail[20], and layer specific *in vivo* recordings are lacking.

In this study, to identify key cell populations involved in associative memory processing, we used *Fos*$^{2A\text{-}iCreERT2}$ (TRAP2[21]) mice to label putative OiP memory engram cells, focussing on association cortices. OiP produced robust TRAP2 labelling at memory encoding and Fos activation following retrieval. TRAP2 and Fos double-positive neurons (engram cells which had been reactivated by retrieval) were significantly more numerous in OiP mice compared to controls; this reactivation correlated with memory performance only in dorsal subregions of LEC. Furthermore, chemogenetic inactivation showed LEC TRAP2 cells to be necessary for expression of OiP memory recall. In *ex vivo* LEC brain slices prepared from mice which had just performed memory retrieval, layer 5 (L5) pyramidal TRAP2 neurons showed increased excitability and firing compared to unlabelled neurons. These data suggest a key role for LEC L5 neurons in forming object-place associations, and demonstrate engram cell specific plasticity related to retrieval and updating of object-place associations.

Results

OiP memory performance correlates with reactivation of dorsolateral entorhinal cortex engram cells

TRAP2 mice were crossed with tdTomato (tdTom) Cre reporter *Ai14* mice[22] resulting in Fos-driven, 4-hydroxytamoxifen (4-OHT)-dependent tdTom labelling. Whilst rewarding and aversive experiences produce high levels of labelling and reactivation at recall in TRAP mice[23,24], it is unknown whether every day, spontaneous learning behaviours such as associative recognition memory are processed in the same manner. TRAP2-Ai14 littermates were assigned to one of two experimental groups: OiP or familiar arena (FA), the latter of which served as the control group (Fig 1A). Mice assigned to the OiP group preferentially explored reconfigured objects when tested at 5 min and 7 d, demonstrating intact memory (S1A).

We focussed our analysis of TRAP2 cell activation and reactivation on two cortical regions known to be essential for associative recognition memory: LEC[13,16,17,25] and mPFC[26,27]. Mice which had not received 4-OHT showed negligible tdTom labelling (Fig S1B). Analysis of cell activation patterns across the whole of mPFC and LEC (Fig 1B) revealed the number of tdTom labelled cells was not significantly different between the OiP and FA conditions in either brain region (Fig 1C, Table S1), however the number of Fos immunostained cells following recall at 7 d was significantly higher in OiP compared to FA mice (Fig 1C, Table S1) and, critically, the percentage of Fos-immunostained tdTom cells (indicating reactivation) was significantly higher in the OiP condition compared to FA in both brain regions (Fig 1C, Table S1) . These same patterns of activation and reactivation were also seen when mPFC was separated into prelimbic (PrL) and infralimbic cortex (IL) subdivisions and the LEC into dorsal lateral (DLent), dorsal intermediate (DIent) and ventral intermediate (VIent) subdivisions (Fig 1D; S1C, Table S1).

To investigate the relationship between memory performance in the OiP task and engram cell reactivation, a Pearson correlation coefficient was computed for each brain region. No significant correlation was found between the combined discrimination ratio (DR) and tdTom cell reactivation in mPFC, nor the PrL and IL subdivisions (Fig 1E, S1D). Analysis of LEC also showed a non-significant trend towards positive correlation between memory performance and tdTom cell reactivation (Fig 1E). Interestingly, analysis of LEC subdivisions identified a statistically significant positive correlation in DLent, a positive but not statistically significant correlation in DIent and a non-significant negative relationship in VIent (Fig 1F). DLent may, therefore, be a critical region for OiP memory retrieval.

The superficial and deep layers of LEC are anatomically distinct, with layers 2 & 3 (L2/3) providing input into the hippocampus while layers 5 & 6 (L5/6) receive inputs from the hippocampus and project to non-hippocampal regions[28]. In the whole LEC significantly more tdTom cells were found in L2/3 than L5/6 in both the FA and OiP conditions, whereas memory retrieval produced equal amounts of Fos labelling in L2/3 and L5/6 in both behavioural tasks (Fig 1G). Surprisingly, a significantly higher proportion of deep layer LEC tdTom cells were reactivated by retrieval in both behavioural conditions (Fig 1G). Analysis of LEC subdivisions showed that this activation and reactivation pattern was consistent across all three LEC subdivisions (Fig 1G, S2A,B, Table S2), with the exception of there being no difference in tdTom labelling in different layers of DLent of OiP mice (Fig 1G, Table S2) or in the reactivation of VIent layers in OiP mice (Fig S2, Table S2).

Layer analysis of mPFC as a whole did not reveal any differences in labelling between L2/3 and L5/6 (Fig S2C). In PrL, significantly more tdTom cells were found in L2/3 in both behavioural tasks, however there was no significant difference in Fos labelling or reactivation between layers following memory retrieval (Fig S2D). In IL significantly more tdTom cells were activated in L5/6 in the OiP task, however no significant differences in layer were observed for Fos labelling or reactivation following memory retrieval for either behavioural condition (Fig S2E).

In summary these data show that OiP recall robustly reactivates LEC and mPFC neurons which were activated at encoding, that reactivation of LEC neurons correlates with memory performance with a dorsoventral gradient, and that reactivation is highest in L5/6 LEC neurons, putatively identifying deep layer DLent as a key locus of object-place representations. We next determined the necessity of LEC TRAP2 neurons for memory performance.

Inactivation of LEC TRAP2 cells impairs OiP memory recall

If activity-labelled neurons are to be considered engram cells, in addition to their reactivation by stimuli relevant to the labelling experience, their activity should also be necessary for retrieval of the memory[29]. To test this hypothesis, TRAP2 mice were crossed with Cre-dependent *hM4Di-DREADD* mice to permit chemogenetic inactivation of activated neurons (Fig 2A). Guide cannulae were implanted bilaterally in LEC (Fig 2B), targeting DLent where TRAP2 cell reactivation was significantly correlated with memory performance (Fig 1F). Following recovery from surgery, mice underwent OiP testing before injection with 4-OHT to drive expression of hM4Di in active neurons (Fig 2A). We then assessed the effect of hM4Di-mediated inactivation on memory retrieval by infusing vehicle or CNO into LEC prior to the second test phase, 48 h after labelling neurons.

Mice assigned to both vehicle and CNO groups showed intact memory at the 5 min delay (Fig 2C, vehicle $t_{(9)} = 4.53$, $p = 0.001$; CNO $t_{(9)} = 5.73$, $p = 0.0003$). Critically, however, mice infused with CNO prior to testing at 48 h had impaired memory, while vehicle infused mice had intact memory (Fig 2C, Drug by test phase $F_{(1,18)} = 21.92$, $p = 0.0002$; vehicle: $t_{(9)} = 10.39$, $p = 3.0 \times 10^{-6}$; CNO: $t_{(9)} =$

-1.24, p = 0.12). No difference in exploration levels were found between vehicle and CNO groups at the sample (Fig 2D, $F_{(1,18)} = 0.21$ p = 0.656) or either test phase (Fig 2E drug by test phase $F_{(1,18)} = 4.50$, p = 0.048; vehicle vs CNO, test 1: p = 0.194, test 2: p = 0.862; T1 vs T2, vehicle: $p = 2x10^{-6}$, CNO: p = 0.001). These data demonstrate the necessity of LEC TRAP neurons for successful retrieval of OiP memory, therefore definitively demonstrating their identity as engram neurons.

Object reconfiguration increases excitability of L5 LEC TRAP2 neurons

Material changes in engram neurons are hypothesised to increase the likelihood of their reactivation upon exposure to specific cues. One mechanism by which this can be achieved is by changes in cellular excitability, which may facilitate firing in response to complete, partial or ambiguous cues[30-32] and support consolidation[33,34].

We investigated neuronal excitability in *TRAP2-Ai14* mice 48 h after TRAP labelling by preparing *ex vivo* slices immediately after memory recall (Fig 3A, S3A), focussing on deep-layer LEC neurons, which had shown the highest levels of reactivation by OiP memory recall (Fig 1G). In slices from these mice, tdTom L5 pyramidal neurons exhibited increased firing in response to depolarising current compared to unlabelled neurons (Fig 3A; Table S3). Further analysis of the physiological properties of these neuronal populations showed input resistance was significantly higher in tdTom neurons (Fig 3A, Table S3). Rheobase, a measure related to input resistance and action potential threshold, was lower in tdTom neurons but not statistically different (Fig S3B, Table S3), likely owing to an insignificant trend to a more depolarised action potential threshold in tdTom neurons (Fig S3B, Table S3). Other membrane properties that influence firing, including afterhyperpolarisation potentials[35,36] (AHP), were not significantly different (Fig S3B, Table S3). In addition to increased excitability, tdTom neurons also showed modified action potential dynamics, exhibiting lower amplitude action potentials which had a slower rate of rise than those observed in unlabelled neurons (Fig S3B, Table S3). Collectively these data show that exposure to a novel configuration of engram-related objects elicits changes in the electrophysiological properties of tdTom neurons, resulting in increased excitability and firing rate in response to depolarising stimuli.

Excitability changes were not observed in other cortical engram cells

That tdTom L5 LEC pyramidal neurons are both reactivated and show heightened excitability following exposure to rearranged objects suggests a key role in OiP memory. We next asked whether other neuronal populations activated by OiP memory also undergo changes in cellular excitability. tdTom labelling was found to be abundant in LEC L2a fan cells, which are required for episodic-like[17] and associative memory[19], in *ex vivo* slices from mice exposed to reconfigured objects. However, unlike L5 pyramidal neurons, no differences in spiking or other measures of intrinsic excitability or action potential waveforms were found between tdTom and unlabelled L2a fan cells (Fig 3B, S3C, Table S4).

We next examined excitability of pyramidal neurons in PRH, a major input to LEC which encodes object identity and novelty[37] but which, in contrast to LEC, is not thought to encode object-location associations[12]. Labelling in PRH had a similar pattern to that seen in in LEC: both Fos labelling (Fig S1C) and tdTom cell reactivation (Fig S1E) after retrieval were elevated in OiP mice compared to FA, although reactivation of PRH engram cells was not significantly correlated with memory performance (Fig S1F). tdTom and Fos labelling was higher in PRH L5/6 than L2/3 (Fig S2F) irrespective of task, and reactivation was enhanced in L5/6 compared to L2/3 in OiP mice

only. However, no differences in action potential firing or other electrophysiological parameters between tdTom and unlabelled PRH neurons were observed (Fig S3D, Table S5).

We additionally assessed excitability in mPFC, however no changes in the firing rate nor other electrophysiological measures were found in L5 pyramidal cells (Fig S3E,F, Table S6) or L2/3 pyramidal cells (Fig S3E,G, Table S7). Together these data show that whilst OiP recall results in significant reactivation of tdTom labelled neurons in multiple cortical regions and layers, increases in cellular excitability and action potential dynamics were only found in L5 LEC neurons.

Increased neuronal excitability of TRAP2 LEC L5 pyramidal neurons requires recall of engram-specific cues with associated novel information

We next examined the behavioural conditions required to elicit changes in engram cell excitability. Increased cellular excitability has been suggested as a mechanism either leading to, or resulting from, recruitment to an engram[35,38]; if such changes persist to 48 h after encoding, then these may explain the increased excitability of LEC L5 tdTom neurons. We investigated this possibility by recording from LEC L5 pyramidal neurons 48 h after encoding, without recall prior to slicing (Fig 3C). We found that tdTom and unlabelled cells had equal rates of firing, cellular excitability and action potential properties (Fig 3C, S4A, Table S8). These data show that increased excitability of tdTom LEC L5 pyramidal cells requires re-exposure to the engram objects.

OiP recall in our experiments contains both static and displaced objects, thus the increased excitability of LEC neurons may result from either memory recall or encoding of new information. To determine whether excitability changes could be induced only by recall, mice were re-exposed to the familiar object configuration (previously encountered in test phase 1) immediately prior to slicing (Fig 3D). Re-exposure to this familiar object configuration did not, however, lead to any changes in firing or intrinsic electrophysiological properties (Fig 3D, S4B Table S9), suggesting that retrieval of specific cues in a familiar configuration does not alter engram cell excitability.

These data suggest that changes in intrinsic excitability may be a mechanism by which novel information regarding object locations is integrated into the pre-existing engram as part of a reconsolidation-like process. Alternatively, the increased excitability in tdTom neurons may have been a response to a more general novelty signal created by object reconfiguration. To determine this, we presented mice with a previously unencountered set of objects at test phase 2 (Fig 3E). No difference in firing rate or other measures of cellular excitability were observed in *ex vivo* slices from mice exposed to novel objects, however action potential dynamics showed similar changes (slower rate of rise, smaller amplitude) to those observed in slices from mice which had encountered rearranged engram-related objects (Fig S4C, Table S10). These data demonstrate that whilst a novel object set can alter action potential dynamics, the increased cellular excitability and firing rates observed in response to object reconfiguration are engram-specific and are not a result of a general novelty signal.

Discussion

Memory engrams for associative recognition memories

Recent studies using molecular-genetic activity-labelling have provided considerable support to the notion of memory engrams as cellular substrates of memory[39,40], however these

investigations have, to date, heavily focused on strongly aversive or rewarding behaviours. Here we provide a detailed characterisation of cortical engrams for associative recognition memory, a spontaneous, unrewarded, single-trial form of learning which is critical to our everyday lives. Our results show that OiP produces robust but sparse labelling of neurons in multiple recognition memory associated cortices, and crucially that these neurons were both strongly reactivated by and, in the case of LEC engram neurons, necessary for memory retrieval, thus implicating these cells as engram neurons. These findings demonstrate engram cell recruitment and reactivation as crucial in spontaneous associative recognition memory.

Engrams within LEC

Interestingly we found that memory performance correlated with reactivation of tdTom cells only in LEC, and that this correlation exhibited a dorsal-ventral gradient, with a strong correlation in DLent and no correlation in VIent. These data support the notion that LEC can support object-place associations in contrast with PRH, which is thought to only encode object identity and novelty[12] and in which no correlation was found between reactivation and memory. Within LEC, deep layer neurons showed higher levels of reactivation than superficial neurons, despite similar numbers of superficial and deep neurons being activated overall at encoding and recall; this heightened level of reactivation combined with intrinsic plasticity seen in these neurons implicates deep DLent as a key locus of object-place associations. These neurons are highly anatomically connected with other associative recognition memory regions: feedback inputs from hippocampus to LEC are topographically organised with dorsal hippocampus projecting most strongly to L5 DLent where synapses converge with top-down inputs from mPFC[16,18], forming a bidirectional LEC-mPFC loop which supports item-outcome associations[41]. Whilst previous studies have shown object-place representations in deep LEC[8], most evidence to date has implicated superficial LEC neurons in encoding associative[19] and episodic-like memory[17], and superficial LEC receives termina from both PRH and postrhinal cortex[42] (although it is unknown if these superficial fibres make contacts upon distal apical dendrites of deep layer pyramidal cells). Our data are not mutually exclusive with this view: deep layer LEC neurons project to L2/3 pyramidal neurons, and although LEC engram neuron reactivation was highest in L5/6, reactivation of L2/3 was also increased by OiP compared to FA.

Plasticity of excitability in LEC L5 neurons

The notion that deep LEC may form object-place associations is supported by plasticity of excitability which occurred specifically in LEC L5 TRAP2 pyramidal neurons following exploration of reconfigured objects, which was absent in L2a fan cells, PRH L5, and both L2/3 and L5 mPFC pyramidal neurons. This finding raises the possibility that plasticity of cellular excitability in these neurons may represent a mechanism by which neural object-place representations can be rapidly altered in response to engram-related environmental novelty. Whilst changes in cellular excitability were only found in LEC L5, this is not to say that other plastic changes, such as synaptic plasticity, do not occur in other cell populations[25,43,44].

Two alterations to LEC L5 tdTom cells were found in this study: firstly, increased input resistance, with an accompanying increase in firing upon depolarisation. The mechanisms underlying this change are unknown, however decreased potassium conductance is a potential mechanism[31]; other mechanisms regulating firing rate such as AHP[30,35] were unaltered. Secondly, we observed action potentials had reduced amplitude and rate of rise, likely reflecting decreased voltage-gated sodium channel function which has previously been observed in response to dopaminergic activity[45], which signals novelty in LEC[19].

Increased engram cell excitability was only observed under specific conditions. The absence of plasticity in tdTom cells from mice which did not re-encounter objects before slicing shows that increased excitability either leading to, or resulting from, recruitment to an engram[35,38] either did not occur or was not persistent 48 h later. Furthermore, as we found no electrophysiological difference between engram and non-engram cells it is unlikely that engram recruitment is biased towards a particular subclass of LEC L5 pyramidal cells, which have different electrophysiological phenotypes[28].

Re-exposure to objects in familiar locations did not alter engram cell excitability. Meanwhile, exploration of completely novel objects resulted only in altered action potential dynamics. We hypothesize that a novelty signal, such as release of neuromodulatory transmitter, may be sufficient to induce changes in action potential dynamics in both the novel objects and reconfigured objects groups, but that this novelty signal must be accompanied by strong activation of synapses within the engram network, including from engram cells in neurons from distal regions such as mPFC and hippocampus, to generate a plasticity signal that results in increased firing.

The function of intrinsic plasticity in engram cells is unclear. Evidence suggests that engram cell intrinsic excitability increases during a short temporal window after memory recall, and that these changes facilitate pattern completion[31]. Heightened excitability may therefore act as a (likely temporary) mechanism of updating environmental representations by integrating new information into an established engram via a re-consolidation like process, and may facilitate processes underlying systems consolidation (such as replay events[46]) which facilitate longer term storage of environmental changes in the form of synaptic changes[43,44].

STAR★Methods

Key resources table

REAGENT or RESOURCE	SOURCE	IDENTIFIER
Antibodies		
Chicken anti-mCherry	Abcam	Cat#ab205402; RRID:AB_2722769
Mouse anti-Fos	Hello Bio	Cat#HB8006
Goat anti-mouse Alexa Fluor 488 conjugate	Invitrogen	Cat#A-11029; RRID:AB_2534088
Goat anti-chicken Alexa Fluor 594 conjugate	Abcam	Cat#ab150176 RRID:AB_2716250
Chemicals, peptides, and recombinant proteins		
4-hydroxytamoxifen	Hello Bio	Cat#HB6040
Clozapine-N-oxide	Hello Bio	Cat#HB6149
VECTASHIELD HardSet Antifade Mounting Medium with DAPI	Vector Laboratories	Cat#H-1500
SIGMAFAST 3,3'-Diaminobenzidine tablets	Sigma	Cat#D4418-50SET
VECTASTAIN Elite ABC-HRP Kit, Peroxidase (Standard)	Vector Laboratories	Cat#PK-6100, RRID:AB_2336819
Mouse on Mouse blocking reagent	Vector Laboratories	Cat#MKB-2213
Mowiol 4-88	Sigma	Cat#81381
Experimental models: Organisms/strains		
TRAP2	Jackson Laboratory	RRID:IMSR_JAX:030323
Ai14	Jackson Laboratory	RRID:IMSR_JAX:007914
hM4Di-DREADD	Jackson Laboratory	RRID:IMSR_JAX:026219
Software and algorithms		
WinLTP 3	W.W.Anderson	www.winltp.com [47]
Prism10	GraphPad Software	https://www.graphpad.com/scientific-software/prism/; RRID: SCR_002798
ImageJ	NIH	https://imagej.net; RRID: SCR_003070
MATLAB R2022a	MATHWORKS	https://www.mathworks.com/; RRID: SCR_001622
LJPCalc	S.W.Harden	RRID:SCR_025044
IBM SPSS statistics v28	IBM	www.ibm.com/products/spss-statistics; RRID:SCR_016479
Leica Application Suite X	Leica	RRID:SCR_013673
Original Code	This paper	Available on request
Other		
Single Acute Guide Cannula, 5mm pedestal, cut to 3.5mm below pedestal	P1 technologies	C315GAS-5/SPC
Dummy Cannula to fit 3.5mm C315GAS-5 with no projection	P1 technologies	C315DCS-5/SPC
Locking internal cannula to fit 3.5mm C315GAS-5 with 1mm projection	P1 technologies	C315LIS-5/SPC

Methods

Animals

All animal procedures were conducted in accordance with the United Kingdom Animals (Scientific Procedures) Act (1986) under project licence number PP7058522 and were approved by the University of Bristol Ethical Review Committee. The following strains of mice were used: TRAP2 (Fos$^{2A\text{-}iCreERT2}$): Fos$^{tm2.1(icre/ERT2)Luo}$/J, JAX stock 030323 generated by L.Luo[21]; Ai14 (: B6.Cg-Gt(ROSA)26Sor$^{tm14(CAG\text{-}tdTomato)Hze}$/J, JAX stock 007914 generated by H.Zeng[22]); hM4Di-DREADD (R26-LSL-Gi-DREADD): B6.129-Gt(ROSA)26Sor$^{tm1(CAG\text{-}CHRM4*,\text{-}mCitrine)Ute}$/J, JAX stock 026219 generated by B.Roth and U.Hochgeschwender[48]. Mice were maintained on a reverse 12 h:12 h light:dark cycle (lights on 20:00-08:00) at constant temperature and humidity with *ad libitum* food and water. Home cage enrichment was present in the form of a cylindrical cardboard tube and a cellulose half-dome. Both male and female mice (sex determined by visual inspection of gonads by the animal breeding unit) were used at ≥10 weeks old. Mice were group housed in cages of 2-4 except for experiments involving cannulated hM4Di-DREADD mice which were single housed to prevent chewing of cannulae between cage-mates – for this reason, only male mice were used for these experiments due to increased tolerance of single housing[49].

Surgery

Implantation of bilateral cannulae into LEC was performed under isoflurane general anaesthesia (3% induction, 2-3% maintenance) and secured in a stereotaxic frame using a mouse anaesthesia head holder and non-rupture ear bars (World Precision Instruments; WPI). Ophthalmic ointment was applied to the eyes to prevent drying, the scalp was sterilised with 4% chlorhexidine, and lidocaine (2%, 0.05 ml) was injected subcutaneously to provide local anaesthesia. A scalpel incision was made along the midline of the scalp and craniotomies were performed with a microdrill (WPI) and 0.5 mm burrs (Fine Science Tools). Guide cannula (26G, P1Technologies) were implanted into LEC (AP -3.0mm, ML ±4.2mm, DV -3.2mm relative to bregma) and secured with gentamycin bone cement (DePuy international). The scalp incision was closed with surgical sutures and wound powder applied to the site. Mice were given 0.5 ml subcutaneous glucose saline for hydration. Analgesia was provided via: 1.5 µg intramuscular buprenorphine given at the end of surgery and 0.15 mg meloxicam given orally in a palatable solution of condensed milk 24 h prior to and 24 and 48 h post-surgery. Mice were allowed to recover for 2 weeks before undergoing behavioural procedures.

Behavioural Procedures

Habituation

Mice were habituated to the entire experimental regimen except objects for at least 6 days prior to activity-dependent labelling. All translocation of mice between cages and behavioural apparatus was done using cardboard enrichment tubes[50]. Mice were first transported from the home room to the behavioural room within 2 hours of dark phase onset where they would remain for a similar duration and timing to activity-dependent labelling day. Cage mates were split into individual experimental cages which had the same dimensions, bedding and enrichment as their home cages, and placed in a designated position in a storage rack surrounded by black curtains. Mice were allowed to individually explore the empty arena for 10 min per day of habituation. This was followed by ~3-5 min of handling in a neighbouring room for habituation to injection procedures. TRAP2 x hM4Di-DREADD mice received additional habituation to intracerebral infusions in the form of daily handling and a dummy infusion of saline 7 days prior to activity-

dependent labelling. Following habituation procedures mice remained in their experimental cages in the storage rack for at least 3 hours before being returned to their home cages with cage mates.

Apparatus

Behavioural testing took place in a wooden, open-topped arena (50 cm x 50 cm) with three black and one grey 40 cm high walls, positioned within a sheet-aluminium faraday cage. The floor was covered with sawdust for all experiments. Behaviour was monitored using an overhead digital camera. Objects of approximately 8 x 8 x 8 cm were constructed from Lego (Lego UK) and varied in colour and shape. The bases of the objects were secured to the arena floor using Velcro and covered with sawdust.

Object-in-place behavioural testing

Lego objects were placed in the four corners of the arena ~ 10 cm from the walls. In the sample phase mice were released into the centre of the arena from their cardboard enrichment tube and allowed to explore objects for 10 min. Mice were returned to their experimental cage for a 5 min delay period during which all objects were cleaned with 100% ethanol to remove olfactory cues. Objects were then replaced into the arena with either the left- or right-hand objects exchanging position - starting positions and the side on which objects were reconfigured were counterbalanced between mice. Mice were then returned to the arena for 10 min (test phase 1) and the time spent exploring objects in novel positions was compared to exploration of objects which remained static. Either 7 days or 48h after test phase 1, mice underwent test phase 2 (10 min). Objects were placed in the arena, objects which had switched location in test phase 1 remained stationary while the objects which had been stationary in test phase 1 now switched locations (Fig 1A). Familiar arena mice underwent the identical procedure without objects in the arena.

Activity-dependent neuronal labelling

Immediately following behavioural procedures, mice were taken to the injection room, scruffed and injected intraperitoneally with 50 $mg.kg^{-1}$ 4-hydroxytamoxifen (4-OHT; 70% Z-isomer; Hello Bio). TRAP2 x hM4Di-DREADD mice were briefly anaesthetised with isoflurane before intraperitoneal injection of 4-OHT to allow replacement of dummy cannulae. 4-OHT was dissolved in 100% ethanol (10 $mg.ml^{-1}$) at 37°C for 30 min (briefly vortexed at ~5 min intervals), then diluted 1:2 with a 1:4 mixture of castor:sunflower seed oils (Sigma). The ethanol was evaporated off using a vacuum centrifuge and the resulting 10 $mg.ml^{-1}$ 4-OHT solution used for injection. Mice were immediately returned to their experimental cage following injection and kept in darkness for a minimum of 3 h before being put back into home cages with cage mates and being returned to the home room. Vehicle injected animals received an injection of the castor:sunflower oil mixture at an equivalent volume to what would have been administered if they were injected with 4-OHT.

Chemogenetic silencing of LEC engram neurons

Following activity dependent labelling of OiP neurons, TRAP2 x hM4Di-DREADD mice were given a period of 48 h to allow expression of hM4Di protein; 48 h was chosen to attempt to restrict protein expression to neuronal somata and thus permit inhibition of only LEC engram neurons, whereas at longer delays hM4Di might be expected to accumulate in the presynaptic input to LEC neurons[51]. Following the 48 h delay, mice received intracerebral infusions of Clozapine-N-

oxide (CNO) or vehicle. General infusion procedures were performed as described previously[52]. CNO was dissolved at 30 µM in sterile saline and 0.05% DMSO and infused at a volume of 0.5 µl per site, over a 2 min period. Vehicle infusions consisted of sterile saline and 0.05% DMSO. 15 min after the start of infusion, mice were returned to the behavioural apparatus for 10 min for test phase 2 in which the object pair which had been static at test phase 1 exchanged position, whilst those which had been re-arranged in test phase 1 now remained static (i.e., if the left hand objects had been moved at test phase 1, the right hand objects were moved at test phase 2).

Immunofluorescence staining

Ninety minutes after the start of test phase 2 mice were given an overdose of sodium pentobarbital (20 mg, Euthatal, Rhone Merieux) and then transcardially perfused with 0.1 M phosphate buffer (PB) followed by 4% paraformaldehyde in 0.1 M PB. Brains were removed and post-fixed in 4% paraformaldehyde for 2h and then incubated in 30% sucrose in PB at room temperature overnight. Brains were sectioned in the coronal plain into 40 µm sections with a cryostat. Four serial sets of sections were collected for each brain region of interest and stored in cryopreserve before immunofluorescent staining. Before immunostaining commenced sections were washed 5 times (2 x 30 min at RT, 3 x 10 min at 35°C) in phosphate buffered saline (PBS) to remove cryopreserve. Sections then underwent staining for Fos and tdTomato. Sections were incubated in 1% H_2O_2 in PBS for 30 min and then washed three times in PBS. Sections underwent antigen retrieval by incubating in sodium citrate buffer (10 mM, pH 6.0) at 80°C for 30 min. When sections had cooled down to RT they were washed four times in 0.2% Triton-X 100 in 0.1 M PBS (PBST). Sections were then incubated in mouse-on-mouse blocking buffer (Vector laboratories, 2 drops per 2.5 ml) in PBST for 1 h followed by incubation in blocking buffer (5% normal goat serum and 2.5% bovine serum albumin in PBST) for 1 h. Sections were then incubated in primary antibody solution to Fos (1:1000 mouse anti-Fos) and tdTomato (1:1000 chicken anti-mCherry) in blocking buffer for 48 h at 4°C. Sections were washed 4 times in PBST and then incubated in secondary antibody solution (1:250 goat-anti mouse Alexa Fluor 488 conjugate and 1:500 goat anti-chicken Alexa Fluor 594 conjugate in blocking buffer) for 24 h at 4°C. Sections were washed four times in PBST and then mounted onto polylysine coated slides. Sections were dried for 24 h in the dark and then coverslipped using Vectashield with DAPI .

Electrophysiological analysis of engram TRAP2 cell excitability

48 h after activity dependent labelling of TRAP2-Ai14 mice, mice underwent test phase 2 (except Fig 3A). Mice were then transported to a slicing room in their experimental cage covered with a black plastic bag and acute *ex vivo* brain slices were prepared. Approximately 10 minutes elapsed between the end of test 2 and the onset of slice preparation.

Acute slice preparation

Mice were anaesthetised with isoflurane (3%) and tested for absence of hind paw pain reflex and eye-blink reflex before decapitation. The brain was rapidly dissected and placed into a beaker of ice-cold sucrose (in mM: 189 sucrose, 26 $NaHCO_3$, 10 D-glucose, 5 $MgSO_4$, 3 KCl, 1.25 NaH_2PO_4, 0.2 $CaCl_2$; Fisher Scientific) bubbled with 95% O_2/5% CO_2. The cerebellum was removed with a scalpel and a coronal cut was made at the approximate rostro-caudal level of the thalamus. The brain was affixed to the tissue stage of a vibratome (7000smz-2, Campden Instruments) with cyanoacrylate glue. 300 µm thick coronal brain slices were made and placed in artificial cerebrospinal fluid (aCSF; in mM: 124 NaCl, 26 $NaHCO_3$, 10 D-glucose, 3 KCl, 2 $CaCl_2$, 1.25

NaH_2PO_4, 1 $MgSO_4$) bubbled with 95% O_2/5% CO_2. Slices were incubated for 1 hr at 34°C and then subsequently at room temperature until use. Recordings began 1 hr after slicing.

Electrophysiological recording

Coronal slices were placed into a submerged recording chamber perfused with 34°C aCSF at a rate of 2ml.min^{-1} and immobilised using a slice anchor (Warner Instruments). Anterior-posterior depth was determined using a brain atlas[53] under a 4x objective and wide field oblique infra-red optics. Neurons were imaged using a 40x immersion objective and oblique infra-red and fluorescence imaging. tdTom neurons were matched with neighbouring unlabelled neurons with similar morphology in the same layer and region of the slice, typically 30-100 µm from each other. Recordings were acquired using either simultaneous dual whole-cell patch clamp or sequential single cell recordings. LEC and perirhinal cortex cellular location was determined using a brain atlas[53]; L5 neurons were 125-300 µm from the white matter, fan cells were in L2a which was visible as a dense cell layer adjacent to the almost acellular region in L1 which extended ~100 µm from the pial surface[17]. mPFC L2/3 and L5 were defined as 125-325 µm and 325-650 µm from the pial surface of PrL, respectively[54].

Whole-cell current-clamp recordings were made using borosilicate glass micropipettes (3–6 MΩ; GC150-10F, Harvard Apparatus) filled with potassium gluconate intracellular solution (in mM: 125 K-gluconate, 40 HEPES, 2 NaCl, 2 MgATP, 0.3 NaGTP, 0.2 EGTA, 0.25% Biocytin, 290-300 mOsm). Series resistance was 10-30 MΩ and was not compensated. Data was obtained with a Multiclamp 700A amplifier (Molecular Devices), digitized at 40 kHz (National Instruments USB-6341) and low-pass filtered at 4 kHz using WinLTP3.00 software[47].

Resting membrane potential (RMP) was recorded immediately after break-in. Subsequently, constant-current was applied to keep cells at approximately -70 mV. Liquid junction potential was calculated to be 16.4 mV using LJPCalc and was not corrected. To assess subthreshold membrane properties and firing properties, cells were injected with a series of 500 ms square wave pulses ranging from -100 to +300 pA. To determine rheobase, cells were injected with an 800 ms linear current ramp to an amplitude sufficient to elicit at least one action potential. To evoke afterdepolarisation potentials (ADP), cells were injected with a 1-2 ms duration square current of 1000-4000 pA amplitude such that a single action potential was evoked. To evoke AHP, neurons were injected with 10 current pulses (1-2 ms duration, 1000-4000 pA amplitude) at 50 Hz. Cells were held for ~15 min in the whole cell configuration before slow withdrawal of the recording electrode to pull an outside-out patch to aid biocytin reconstruction. The location of neurons with respect to each other was recorded to assist in identifying biocytin stained neurons.

Immunohistochemical biocytin staining

Following recording, slices were fixed in 4% paraformaldehyde in 0.1 M PB overnight and subsequently stored in 0.1 M PB until staining. Slices were washed 6 x 10 min in PB, then incubated in 3% H_2O_2 in PB for 30 min to block endogenous peroxidase activity, then washed again as above before incubation in 1% (vol/vol) avidin–biotinylated HRP complex (ABC) in PB containing 0.1% (vol/vol) Triton X-100 at RT for 3 hrs. Slices were then washed as above before incubation in 3,3'-diaminobenzidine solution for 5-10 min until staining of neuronal structures was visible. The reaction was stopped by transferring slices to cold PB, followed by further washing as above. Slices were mounted, coverslipped using Mowiol 4-88 mounting media and allowed to dry overnight before imaging.

Exclusion and classification criteria

Biocytin-immunohistochemistry was used to make post-hoc corrections to cell location (layer, subregion) and morphology where neurons had been mis-labelled at the time of recording. Pyramidal neurons had primary apical dendrites projecting towards the pia mater, whilst L2 fan cells had a characteristic broad dendritic arbor extending into L1[17,55]. Neurons were excluded from analysis if their RMP exceeded -50 mV, membrane potential became persistently unstable or series resistance exceeded 30 MΩ. Individual electrophysiological sweeps were excluded where membrane potential was transiently unstable, deviated from -70 mV, or spontaneous activity prevented accurate measurement of data.

Quantification and statistical analysis

Behaviour scoring and statistics

Exploratory behaviour was manually scored and defined as the animal directing its nose towards the object at a distance of <2 cm and actively exploring the object. Any other behaviour, such as looking around while sitting on or resting against the object, grooming within 2 cm of an object, or digging at object bases, was not considered object exploration. Discrimination between the objects was calculated using a discrimination ratio (DR), calculated as the absolute difference in the time spent exploring the moved and unmoved stimuli divided by the time spent exploring all the objects. The DR takes into account individual differences in the total amount of object exploration[56,57]. For the combined DR the exploration of the moved stimuli in test phase one and two was added together and the same was done for the unmoved stimuli and these combined values were used to calculate the combined DR. Performance in each test phase and for the combined DR was assessed using a two-tailed one-sample t-test against chance (DR = 0). Exploration across the phases of the task were compared using a one-way within subjects ANOVA. Post-hoc comparisons used a Bonferroni correction. For chemogenetic silencing of engram cells in LEC, DR and total object exploration levels across test phase 1 and 2 was compared using a two-way ANOVA with drug as a between subjects factor and test phase as a within subjects factor. Post-hoc comparisons examined simple main effects. Comparison of exploration in the sample phase used a one-way between subjects ANOVA. Performance in the test phases was assessed against chance using a one-sample t-test as previously described.

Cell counting protocol and statistics

For the quantification of tdTom, Fos and DAPI expression in mPFC, LEC and PRH, cells were counted bilaterally from 4 (mPFC) or 5 (LEC and PRH) coronal sections from specific locations along the anterior-posterior length of each brain region (Table S11). Fluorescent images were acquired using a Leica Microsystems DM6 B microscope and Hamamatsu C13400-20CU Digital CMOS camera via the Leica Application Suite X software using 100x magnification. Manual cell counting was performed using ImageJ software. Images were split into individual channels. For each cortical area, a region of interest (ROI; 0.5 mm (height) by 0.25 mm (width)) was placed over layer 2/3 and layer 5/6 using the DAPI channel in each slice. Cortical regions were identified using a brain atlas[53]. Cell counts for each channel were obtained as follows; background subtraction was applied to remove background noise, thresholds were set and images were converted to binary. The analyse particles tool was used to quantify the number of labelled cells in each ROI based on particle size (50-500 μm^2 tdTom, 20-150 μm^2 Fos) and circularity (0.4-1.0). Overlap between tdTom and Fos expression was determined by digitally merging the analysed images for each ROI to form a composite image and the number of co-labelled cells quantified. All cell counting was performed by an experimenter blind to the behavioural condition of each animal.

To analyse each brain subregion, cell counts in L2/3 and L5/6 ROIs were combined for each hemisphere, the counts for each hemisphere and for each AP depth counted were averaged. To generate counts for all of mPFC and LEC, the counts for the individual subregions were averaged in each animal to generate counts for the whole brain region. To generate counts for L2/3 and L5/6 of cortex, counts in each region were averaged across hemispheres and sections. These averaged counts were then converted into counts per mm^2. Percent overlap was calculated as ($tdTom^+Fos^+$ cells/$tdTom^+$ cells) * 100.

Comparisons of cell counts across the whole cortical regions between behavioural conditions used a one-way ANOVA with behavioural condition as a between subject factor. Comparison of layer 2/3 and layer 5/6 counts between behavioural conditions used a two-way ANOVA with cortical depth as a within subjects factor and behavioural condition as a between subjects factor. Post-hoc tests analysed simple main effects where appropriate. To analyse the relationship between memory performance and cell reactivation a Pearson's correlation coefficient was calculated comparing combined DR and % reactivation. All statistical analyses were performed using SPSS and significance was set at $p < 0.05$.

Electrophysiology statistics

Electrophysiological data were imported into MATLAB for analysis using custom-written scripts based upon Kerrigan et al. 2014[58] (code available on request). Action potential parameters are measured from the first action potential from the smallest square-wave current-injection which yielded an action potential. Reported input resistance values are steady-state input resistance. Statistical analysis of all electrophysiological variables was performed in GraphPad Prism 10 using Mann Whitney U test, except action potential firing where a mixed-effect model with a Greenhouse-Geisser correction applied and labelling and current injection as factors was used, and ADP presence where a Chi-squared test was used. Cells were considered the experimental unit for electrophysiology.

Additional resources

Data and code used in this manuscript are available upon request. Generative AI was not used in any aspect of this work.

Acknowledgements

This work was supported by a Wellcome Trust Joint Investigator Award to E.C.W. and Z.I.B. (206401/Z/17/Z), a BBSRC project grant to Z.I.B., E.C.W and P.J.B. (BB/X000915/1) and a BBSRC project grant to E.C.W and G.R.I.B. (BB/Y006402/1). We thank Dr Emma Cahill for helpful comments on the manuscript.

Author Contributions

Conceptualization and methodology, P.J.B., G.R.I.B., E.C.W. and Z.I.B.; investigation, P.J.B., G.R.I.B., C.A.B. and L.K.; data analysis, P.J.B., G.R.I.B. and C.A.B.; Writing – original draft, P.J.B.; review and editing, P.J.B., G.R.I.B., C.A.B., E.C.W. and Z.I.B.; Supervision, E.C.W. and Z.I.B.; Funding acquisition, P.J.B., G.R.I.B., E.C.W. and Z.I.B.

Declaration of Interests

The authors declare no competing interests. Generative AI was not used for any aspect of this manuscript.

References

1. Aggleton, J.P., and Nelson, A.J.D. (2020). Distributed interactive brain circuits for object-in-place memory: A place for time? Brain Neurosci Adv *4*, 2398212820933471. 10.1177/2398212820933471.
2. Ennaceur, A., Neave, N., and Aggleton, J. (1997). Spontaneous object recognition and object location memory in rats: the effects of lesions in the cingulate cortices, the medial prefrontal cortex, the cingulum bundle and the fornix. Exp Brain Res *113*, 509-519.
3. Barker, G.R.I., Bird, F., Alexander, V., and Warburton, E.C. (2007). Recognition Memory for Objects, Place, and Temporal Order: A Disconnection Analysis of the Role of the Medial Prefrontal Cortex and Perirhinal Cortex. J. Neurosci. *27*, 2948-2957. 10.1523/jneurosci.5289-06.2007.
4. Eichenbaum, H., Yonelinas, A.P., and Ranganath, C. (2007). The Medial Temporal Lobe and Recognition Memory. Annual Review of Neuroscience *30*, 123-152. doi:10.1146/annurev.neuro.30.051606.094328.
5. Nilssen, E.S., Doan, T.P., Nigro, M.J., Ohara, S., and Witter, M.P. (2019). Neurons and networks in the entorhinal cortex: A reappraisal of the lateral and medial entorhinal subdivisions mediating parallel cortical pathways. Hippocampus *29*, 1238-1254. 10.1002/hipo.23145.
6. Wang, C., Chen, X., and Knierim, J.J. (2020). Egocentric and allocentric representations of space in the rodent brain. Curr Opin Neurobiol *60*, 12-20. 10.1016/j.conb.2019.11.005.
7. Deshmukh, S.S., and Knierim, J.J. (2011). Representation of non-spatial and spatial information in the lateral entorhinal cortex. Front Behav Neurosci *5*, 69. 10.3389/fnbeh.2011.00069.
8. Keene, C.S., Bladon, J., McKenzie, S., Liu, C.D., O'Keefe, J., and Eichenbaum, H. (2016). Complementary Functional Organization of Neuronal Activity Patterns in the Perirhinal, Lateral Entorhinal, and Medial Entorhinal Cortices. J Neurosci *36*, 3660-3675. 10.1523/JNEUROSCI.4368-15.2016.
9. Wang, C., Lee, H., Rao, G., and Knierim, J.J. (2024). Multiplexing of temporal and spatial information in the lateral entorhinal cortex. Nat Commun *15*, 10533. 10.1038/s41467-024-54932-5.
10. Wang, C., Chen, X., Lee, H., Deshmukh, S.S., Yoganarasimha, D., Savelli, F., and Knierim, J.J. (2018). Egocentric coding of external items in the lateral entorhinal cortex. Science *362*, 945-949. 10.1126/science.aau4940.
11. Tsao, A., Sugar, J., Lu, L., Wang, C., Knierim, J.J., Moser, M.B., and Moser, E.I. (2018). Integrating time from experience in the lateral entorhinal cortex. Nature *561*, 57-62. 10.1038/s41586-018-0459-6.
12. Deshmukh, S.S., Johnson, J.L., and Knierim, J.J. (2012). Perirhinal cortex represents nonspatial, but not spatial, information in rats foraging in the presence of objects: comparison with lateral entorhinal cortex. Hippocampus *22*, 2045-2058. 10.1002/hipo.22046.
13. Wilson, D.I., Watanabe, S., Milner, H., and Ainge, J.A. (2013). Lateral entorhinal cortex is necessary for associative but not nonassociative recognition memory. Hippocampus *23*, 1280-1290. 10.1002/hipo.22165.
14. Van Cauter, T., Camon, J., Alvernhe, A., Elduayen, C., Sargolini, F., and Save, E. (2013). Distinct roles of medial and lateral entorhinal cortex in spatial cognition. Cereb Cortex *23*, 451-459. 10.1093/cercor/bhs033.

15. Chao, O.Y., Huston, J.P., Li, J.S., Wang, A.L., and de Souza Silva, M.A. (2016). The medial prefrontal cortex-lateral entorhinal cortex circuit is essential for episodic-like memory and associative object-recognition. Hippocampus *26*, 633-645. 10.1002/hipo.22547.
16. Kinnavane, L., Barker, G.R.I., Banks, P.J., Bashir, Z.I., and Warburton, E.C. (2025). Medial prefrontal cortex input to lateral entorhinal cortex supports both encoding and retrieval of associative recognition memory. BioRxiv. 10.1101/2025.08.14. 670409
17. Vandrey, B., Garden, D.L.F., Ambrozova, V., McClure, C., Nolan, M.F., and Ainge, J.A. (2020). Fan Cells in Layer 2 of the Lateral Entorhinal Cortex Are Critical for Episodic-like Memory. Curr Biol *30*, 169-175 e165. 10.1016/j.cub.2019.11.027.
18. Kinnavane, L., and Banks, P.J. (2022). Ex Vivo Optogenetic Interrogation of Long-Range Synaptic Transmission and Plasticity from Medial Prefrontal Cortex to Lateral Entorhinal Cortex. J Vis Exp. 10.3791/63077.
19. Lee, J.Y., Jun, H., Soma, S., Nakazono, T., Shiraiwa, K., Dasgupta, A., Nakagawa, T., Xie, J.L., Chavez, J., Romo, R., et al. (2021). Dopamine facilitates associative memory encoding in the entorhinal cortex. Nature *598*, 321-326. 10.1038/s41586-021-03948-8.
20. Barbosa, F.F., Santos, J.R., Meurer, Y.S., Macedo, P.T., Ferreira, L.M., Pontes, I.M., Ribeiro, A.M., and Silva, R.H. (2013). Differential Cortical c-Fos and Zif-268 Expression after Object and Spatial Memory Processing in a Standard or Episodic-Like Object Recognition Task. Front Behav Neurosci *7*, 112. 10.3389/fnbeh.2013.00112.
21. Allen, W.E., DeNardo, L.A., Chen, M.Z., Liu, C.D., Loh, K.M., Fenno, L.E., Ramakrishnan, C., Deisseroth, K., and Luo, L. (2017). Thirst-associated preoptic neurons encode an aversive motivational drive. Science *357*, 1149-1155. 10.1126/science.aan6747.
22. Madisen, L., Zwingman, T.A., Sunkin, S.M., Oh, S.W., Zariwala, H.A., Gu, H., Ng, L.L., Palmiter, R.D., Hawrylycz, M.J., Jones, A.R., et al. (2010). A robust and high-throughput Cre reporting and characterization system for the whole mouse brain. Nat Neurosci *13*, 133-140. 10.1038/nn.2467.
23. DeNardo, L.A., Liu, C.D., Allen, W.E., Adams, E.L., Friedmann, D., Fu, L., Guenthner, C.J., Tessier-Lavigne, M., and Luo, L. (2019). Temporal evolution of cortical ensembles promoting remote memory retrieval. Nat Neurosci *22*, 460-469. 10.1038/s41593-018-0318-7.
24. Bobadilla, A.C., Dereschewitz, E., Vaccaro, L., Heinsbroek, J.A., Scofield, M.D., and Kalivas, P.W. (2020). Cocaine and sucrose rewards recruit different seeking ensembles in the nucleus accumbens core. Mol Psychiatry *25*, 3150-3163. 10.1038/s41380-020-00888-z.
25. Tozzi, F., Guglielmo, S., Paraciani, C., van den Oever, M.C., Mainardi, M., Cattaneo, A., and Origlia, N. (2024). Involvement of a lateral entorhinal cortex engram in episodic-like memory recall. Cell Rep *43*, 114795. 10.1016/j.celrep.2024.114795.
26. Barker, G.R., Banks, P.J., Scott, H., Ralph, G.S., Mitrophanous, K.A., Wong, L.F., Bashir, Z.I., Uney, J.B., and Warburton, E.C. (2017). Separate elements of episodic memory subserved by distinct hippocampal-prefrontal connections. Nat Neurosci *20*, 242-250. 10.1038/nn.4472.
27. Preston, A.R., and Eichenbaum, H. (2013). Interplay of hippocampus and prefrontal cortex in memory. Curr Biol *23*, R764-773. 10.1016/j.cub.2013.05.041.
28. Ohara, S., Blankvoort, S., Nair, R.R., Nigro, M.J., Nilssen, E.S., Kentros, C., and Witter, M.P. (2021). Local projections of layer Vb-to-Va are more prominent in lateral than in medial entorhinal cortex. Elife *10*. 10.7554/eLife.67262.
29. Tanaka, K.Z., Pevzner, A., Hamidi, A.B., Nakazawa, Y., Graham, J., and Wiltgen, B.J. (2014). Cortical representations are reinstated by the hippocampus during memory retrieval. Neuron *84*, 347-354. 10.1016/j.neuron.2014.09.037.

30. Cai, D.J., Aharoni, D., Shuman, T., Shobe, J., Biane, J., Song, W., Wei, B., Veshkini, M., La-Vu, M., Lou, J., et al. (2016). A shared neural ensemble links distinct contextual memories encoded close in time. Nature *534*, 115-118. 10.1038/nature17955.
31. Pignatelli, M., Ryan, T.J., Roy, D.S., Lovett, C., Smith, L.M., Muralidhar, S., and Tonegawa, S. (2019). Engram Cell Excitability State Determines the Efficacy of Memory Retrieval. Neuron *101*, 274-284 e275. 10.1016/j.neuron.2018.11.029.
32. Whitaker, L.R., Warren, B.L., Venniro, M., Harte, T.C., McPherson, K.B., Beidel, J., Bossert, J.M., Shaham, Y., Bonci, A., and Hope, B.T. (2017). Bidirectional Modulation of Intrinsic Excitability in Rat Prelimbic Cortex Neuronal Ensembles and Non-Ensembles after Operant Learning. J Neurosci *37*, 8845-8856. 10.1523/JNEUROSCI.3761-16.2017.
33. Zhang, W., and Linden, D.J. (2003). The other side of the engram: experience-driven changes in neuronal intrinsic excitability. Nat Rev Neurosci *4*, 885-900. 10.1038/nrn1248.
34. Thompson, L.T., Moyer, J.R., Jr., and Disterhoft, J.F. (1996). Transient changes in excitability of rabbit CA3 neurons with a time course appropriate to support memory consolidation. J Neurophysiol *76*, 1836-1849. 10.1152/jn.1996.76.3.1836.
35. Disterhoft, J.F., and Oh, M.M. (2006). Learning, aging and intrinsic neuronal plasticity. Trends Neurosci *29*, 587-599. 10.1016/j.tins.2006.08.005.
36. Whitaker, L.R., Warren, B.L., Venniro, M., Harte, T.C., McPherson, K.B., Beidel, J., Bossert, J.M., Shaham, Y., Bonci, A., and Hope, B.T. (2017). Bidirectional Modulation of Intrinsic Excitability in Rat Prelimbic Cortex Neuronal Ensembles and Non-Ensembles after Operant Learning. Journal of Neuroscience *37*, 8845-8856. 10.1523/JNEUROSCI.3761-16.2017.
37. Seoane, A., Tinsley, C.J., and Brown, M.W. (2012). Interfering with Fos expression in rat perirhinal cortex impairs recognition memory. Hippocampus. 10.1002/hipo.22028.
38. Josselyn, S.A., and Frankland, P.W. (2018). Memory Allocation: Mechanisms and Function. Annu Rev Neurosci *41*, 389-413. 10.1146/annurev-neuro-080317-061956.
39. Ortega-de San Luis, C., Pezzoli, M., Urrieta, E., and Ryan, T.J. (2023). Engram cell connectivity as a mechanism for information encoding and memory function. Curr Biol *33*, 5368-5380 e5365. 10.1016/j.cub.2023.10.074.
40. Josselyn, S.A., and Tonegawa, S. (2020). Memory engrams: Recalling the past and imagining the future. Science *367*. 10.1126/science.aaw4325.
41. Jun, H., Lee, J.Y., Bleza, N.R., Ichii, A., Donohue, J.D., and Igarashi, K.M. (2024). Prefrontal and lateral entorhinal neurons co-dependently learn item-outcome rules. Nature *633*, 864-871. 10.1038/s41586-024-07868-1.
42. Doan, T.P., Lagartos-Donate, M.J., Nilssen, E.S., Ohara, S., and Witter, M.P. (2019). Convergent Projections from Perirhinal and Postrhinal Cortices Suggest a Multisensory Nature of Lateral, but Not Medial, Entorhinal Cortex. Cell Rep *29*, 617-627 e617. 10.1016/j.celrep.2019.09.005.
43. Ryan, T.J., Roy, D.S., Pignatelli, M., Arons, A., and Tonegawa, S. (2015). Memory. Engram cells retain memory under retrograde amnesia. Science *348*, 1007-1013. 10.1126/science.aaa5542.
44. Lee, J.H., Kim, W.B., Park, E.H., and Cho, J.H. (2023). Neocortical synaptic engrams for remote contextual memories. Nat Neurosci *26*, 259-273. 10.1038/s41593-022-01223-1.
45. Cantrell, A.R., and Catterall, W.A. (2001). Neuromodulation of Na+ channels: an unexpected form of cellular plasticity. Nat Rev Neurosci *2*, 397-407. 10.1038/35077553.
46. Olafsdottir, H.F., Bush, D., and Barry, C. (2018). The Role of Hippocampal Replay in Memory and Planning. Curr Biol *28*, R37-R50. 10.1016/j.cub.2017.10.073.
47. Anderson, W.W., and Collingridge, G.L. (2007). Capabilities of the WinLTP data acquisition program extending beyond basic LTP experimental functions. J Neurosci Methods *162*, 346-356. 10.1016/j.jneumeth.2006.12.018.

48. Zhu, H., Aryal, D.K., Olsen, R.H., Urban, D.J., Swearingen, A., Forbes, S., Roth, B.L., and Hochgeschwender, U. (2016). Cre-dependent DREADD (Designer Receptors Exclusively Activated by Designer Drugs) mice. Genesis *54*, 439-446. 10.1002/dvg.22949.
49. Davies, J.J., M.G.; Hinchcliffe, J.K.; Mendl, M.; Robinson, E.S.J. (2025). Male mice prefer to live on their own. BioRxiv, 21. 10.1101/2025.05.02.651815.
50. Davies, J.R., Purawijaya, D.A., Bartlett, J.M., and Robinson, E.S.J. (2022). Impact of Refinements to Handling and Restraint Methods in Mice. Animals (Basel) *12*. 10.3390/ani12172173.
51. Stachniak, T.J., Ghosh, A., and Sternson, S.M. (2014). Chemogenetic synaptic silencing of neural circuits localizes a hypothalamus-->midbrain pathway for feeding behavior. Neuron *82*, 797-808. 10.1016/j.neuron.2014.04.008.
52. Barker, G.R., Bashir, Z.I., Brown, M.W., and Warburton, E.C. (2006). A temporally distinct role for group I and group II metabotropic glutamate receptors in object recognition memory. Learn Mem *13*, 178-186. 10.1101/lm.77806.
53. Paxinos, G., and Franklin, K.B.J. (2019). Paxinos and Franklin's the Mouse Brain in Stereotaxic Coordinates, Compact, 5th Edition (Academic Press).
54. Anastasiades, P.G., Boada, C., and Carter, A.G. (2019). Cell-Type-Specific D1 Dopamine Receptor Modulation of Projection Neurons and Interneurons in the Prefrontal Cortex. Cereb Cortex *29*, 3224-3242. 10.1093/cercor/bhy299.
55. Tahvildari, B., and Alonso, A. (2005). Morphological and electrophysiological properties of lateral entorhinal cortex layers II and III principal neurons. J Comp Neurol *491*, 123-140. 10.1002/cne.20706.
56. Ennaceur, A., and Delacour, J. (1988). A new one-trial test for neurobiological studies of memory in rats. 1: Behavioral data. Behav Brain Res *31*, 47-59.
57. Dix, S., and Aggleton, J. (1999). Extending the spontaneous preference test of recognition: evidence of object-location and object-context recognition. Behav Brain Res *99*, 191-200.
58. Kerrigan, T.L., Brown, J.T., and Randall, A.D. (2014). Characterization of altered intrinsic excitability in hippocampal CA1 pyramidal cells of the Abeta-overproducing PDAPP mouse. Neuropharmacology *79*, 515-524. 10.1016/j.neuropharm.2013.09.004.

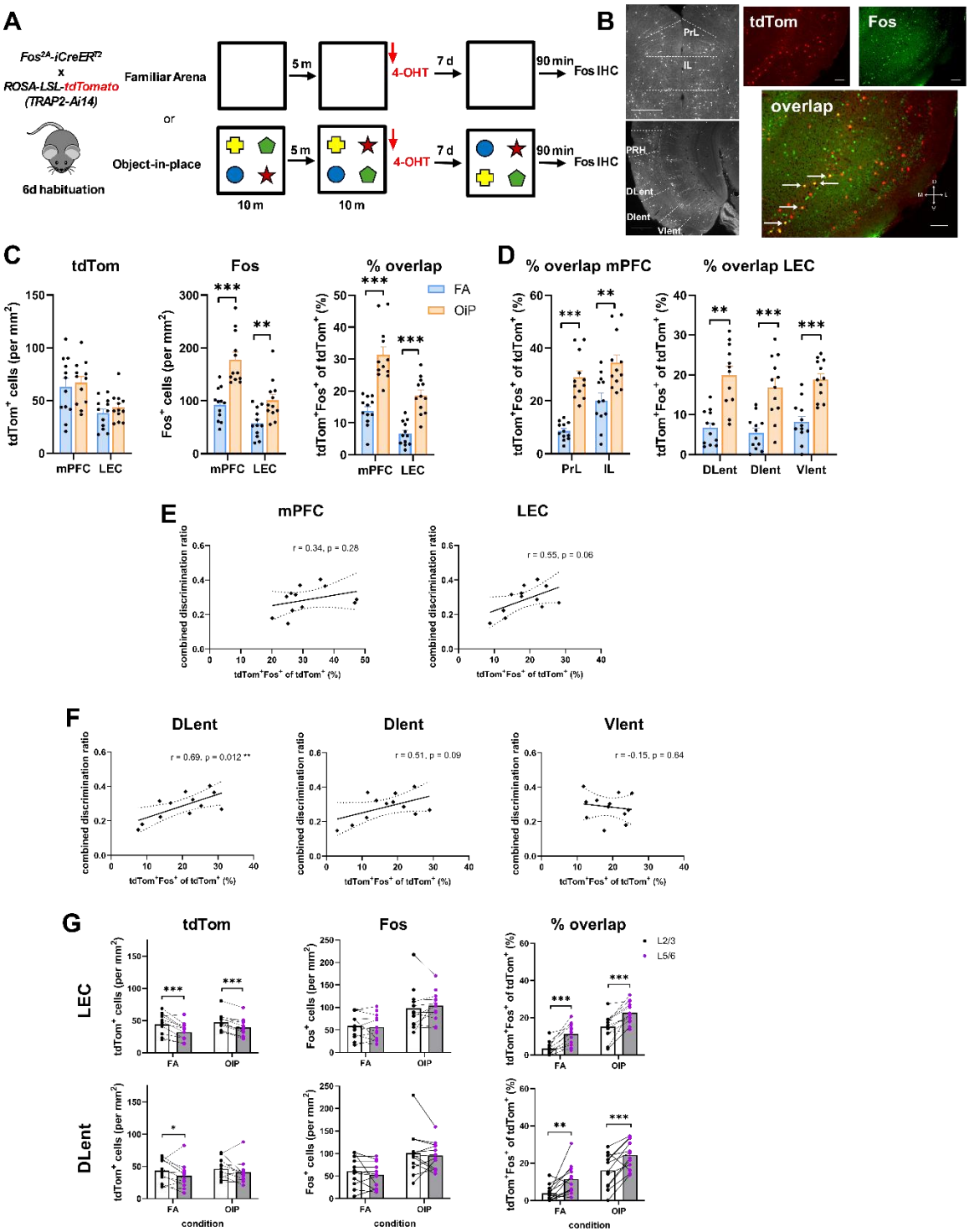

Figure 1: Reactivation of a dorsal lateral entorhinal cortex engram correlates with associative recognition memory performance.

A: Experimental outline for associative memory-induced engram cell labelling.

B: (Left) example OiP induced tdTom labelling in mPFC (upper) and LEC (lower) scale bar: 500 µm. (Right) example tdTom, Fos and overlap in LEC, arrows indicate cells expressing both tdTom and Fos; scale bar: 100 µm.

C: (Left to right) tdTom expression, Fos expression and percent overlap in mPFC and LEC for FA and OiP behavioural conditions.

D: Percent overlap of tdTom and Fos in mPFC subregions PrL and IL and LEC subregions DLent, DIent and VIent.

E: Correlation between tdTom/Fos overlap and memory performance (combined discrimination ratio) in OiP behavioural task for mPFC and LEC. Dashed line show 95% confidence intervals.

F: Same as (E) for LEC subregions.

G: Expression levels of tdTom (left), Fos (middle) and overlap (right) in layers 2 & 3 and layers 5 & 6 of LEC (top) and DLent (bottom).

* $p < 0.05$, ** $p < 0.01$, *** $p < 0.001$. N = 12 mice for all experiments. All error bars indicate mean + SEM. See tables S1 and S2 for detailed statistical analysis.

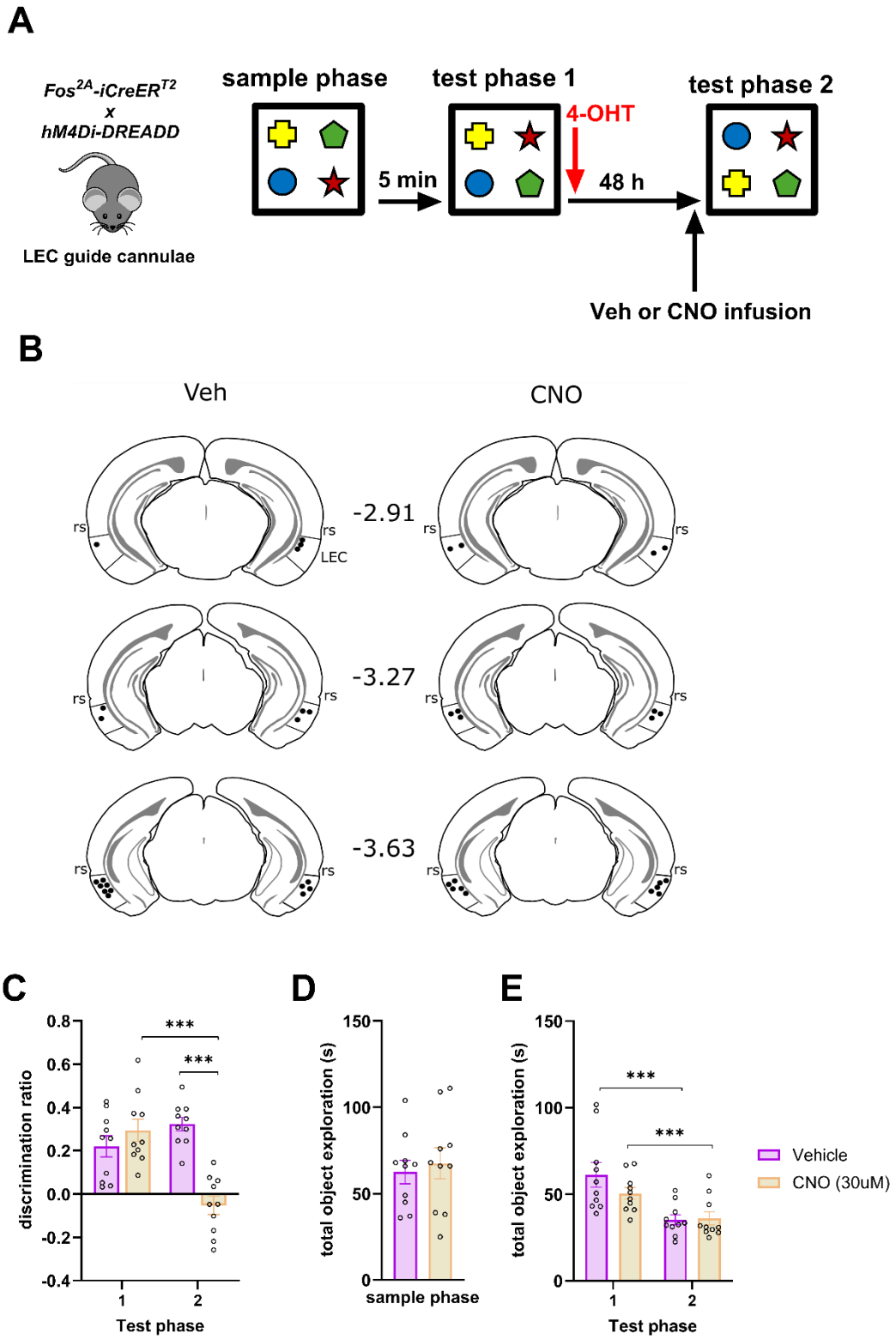

Figure 2: Engram cells in lateral entorhinal cortex are essential for the retrieval of associative recognition memory.

A: Experimental outline for deactivating LEC engram cells during associative recognition memory retrieval.

B: LEC cannula locations (represented by black dots) in the vehicle (left) and CNO (right) infused animals. Numbers represent AP position in mm relative to bregma. rs = rhinal sulcus.

C: Memory performance (discrimination ratio) at test phase 1 and test phase 2 of vehicle and CNO infused animals.

D: Total object exploration during the sample phase of the OiP task.

E: Total object exploration levels during test phase 1 and test phase 2 of the object in place task.

*** p<0.001. N = 10 animals for all conditions. Bars show mean ± SEM. For details of statistical analysis see text.

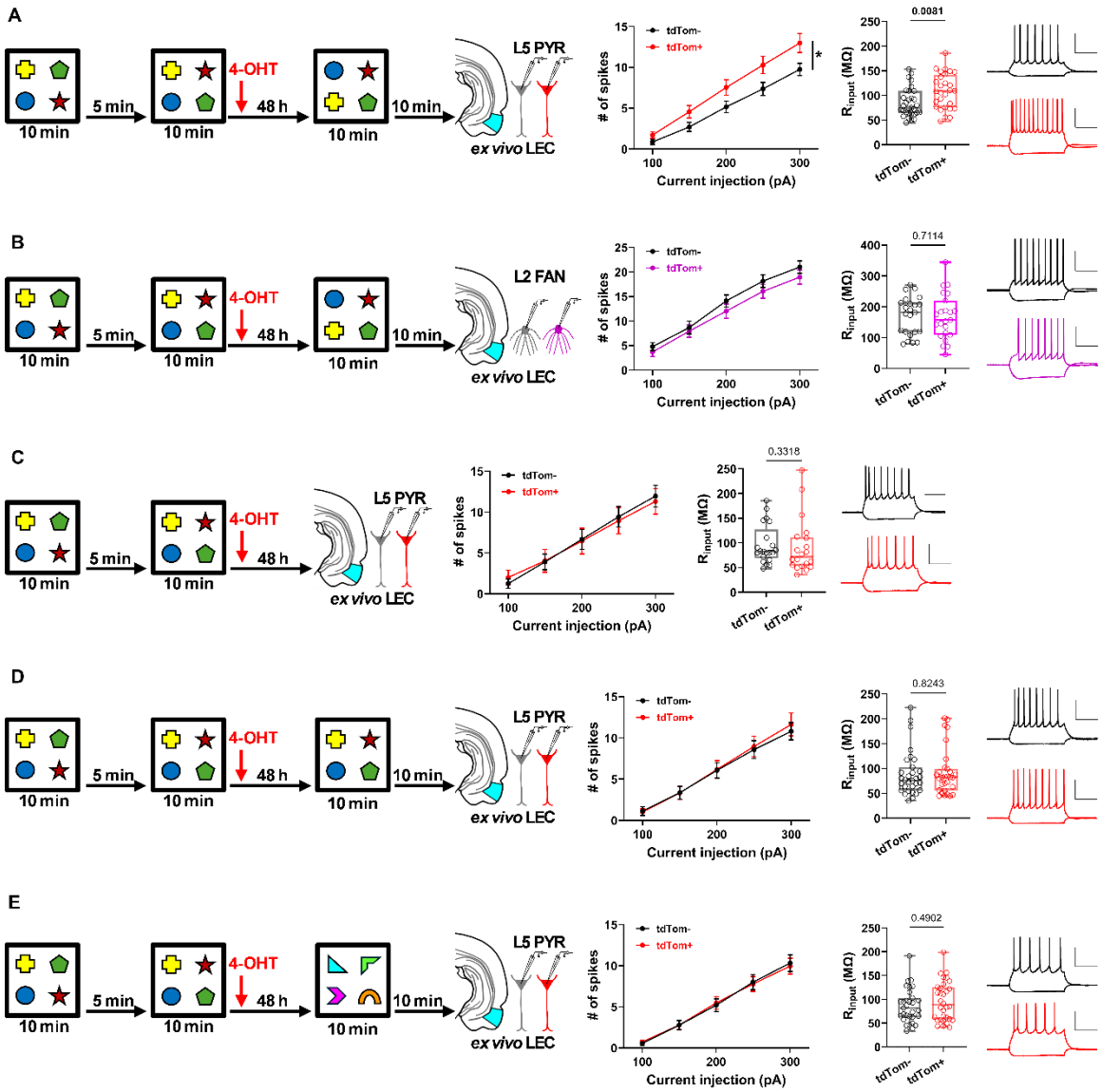

Figure 3. Object reconfiguration increases excitability of LEC L5 pyramidal engram cells

A: (Left) Labelling strategy for *ex vivo* L5 LEC pyramidal cell recordings from animals exposed to reconfigured objects before slicing. (Right) Action potential firing and input resistance of labelled and unlabelled neurons with representative voltage responses to -100 and +200 pA current injections for a tdTom$^-$ and tdTom$^+$ cell pair.

B: Same as (A) but for L2 fan cells.

C: Same as (A) for animals which were not presented with a second test phase before slicing

D: Same as (A) for animals shown a familiar object configuration before slicing.

E: Same as (A) for animals shown a novel object set before slicing. Scale bars 200 ms, 40 mV. * = $p<0.05$.

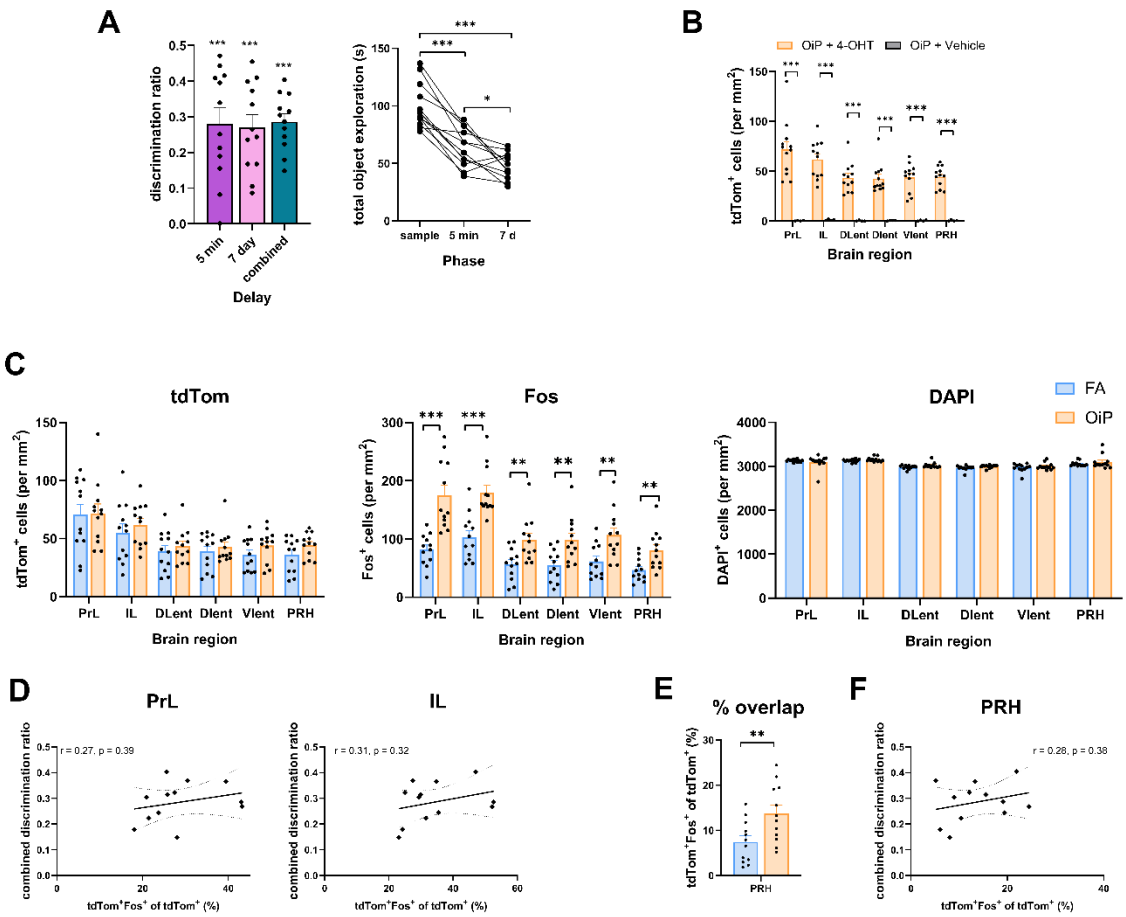

Supplementary Figure 1. Behavioural and labelling data from FA and OiP tasks.

A: (Left) Animals showed significant discrimination between the moved and unmoved objects in the OiP task, as measured by the discrimination ratio, at 5 min and 7 d delays and when combined (5 min $t_{(11)} = 7.55$, $p = 1.15 \times 10^{-5}$; 7 day $t_{(11)} = 6.31$, $p = 5.79 \times 10^{-5}$; combined $t_{(11)} = 12.79$, $p = 6.04 \times 10^{-8}$). (Right) Total object exploration significantly decreased across each phase of the behavioural task ($F_{(2,22)} = 46.99$, $p = 1.14 \times 10^{-8}$, post-hoc sample vs 5 min $p = 2.82 \times 10^{-5}$, sample vs 7 day: $p = 1.91 \times 10^{-5}$, 5 min vs 7 day: $p = 0.032$).

B: Expression of tdTom was dependent on injection of 4-OHT in all brain regions (in each brain region one-way ANOVA $F_{(1,14)} > 28$, $p < 0.001$). OiP + 4-OHT n = 12, OiP + vehicle n = 4.

C: tdTom, Fos and DAPI cell counts in subregions of mPFC and LEC and in PRH for FA and OiP conditions.

D: No significant correlation between tdTom and Fos overlap and memory performance in either PrL or IL subregions of mPFC. Dashed line show 95% confidence intervals.

E: Overlap between tdTom and Fos expression in the perirhinal cortex is significantly higher in the OiP compared to the FA condition.

F: No significant correlation between tdTom and Fos overlap and memory performance in the perirhinal cortex. Dashed line show 95% confidence intervals.

* $p < 0.05$, ** $p < 0.01$, *** $p < 0.001$. For FA vs OiP comparisons n = 12 animals for each condition. See table S1 for detailed statistical analysis.

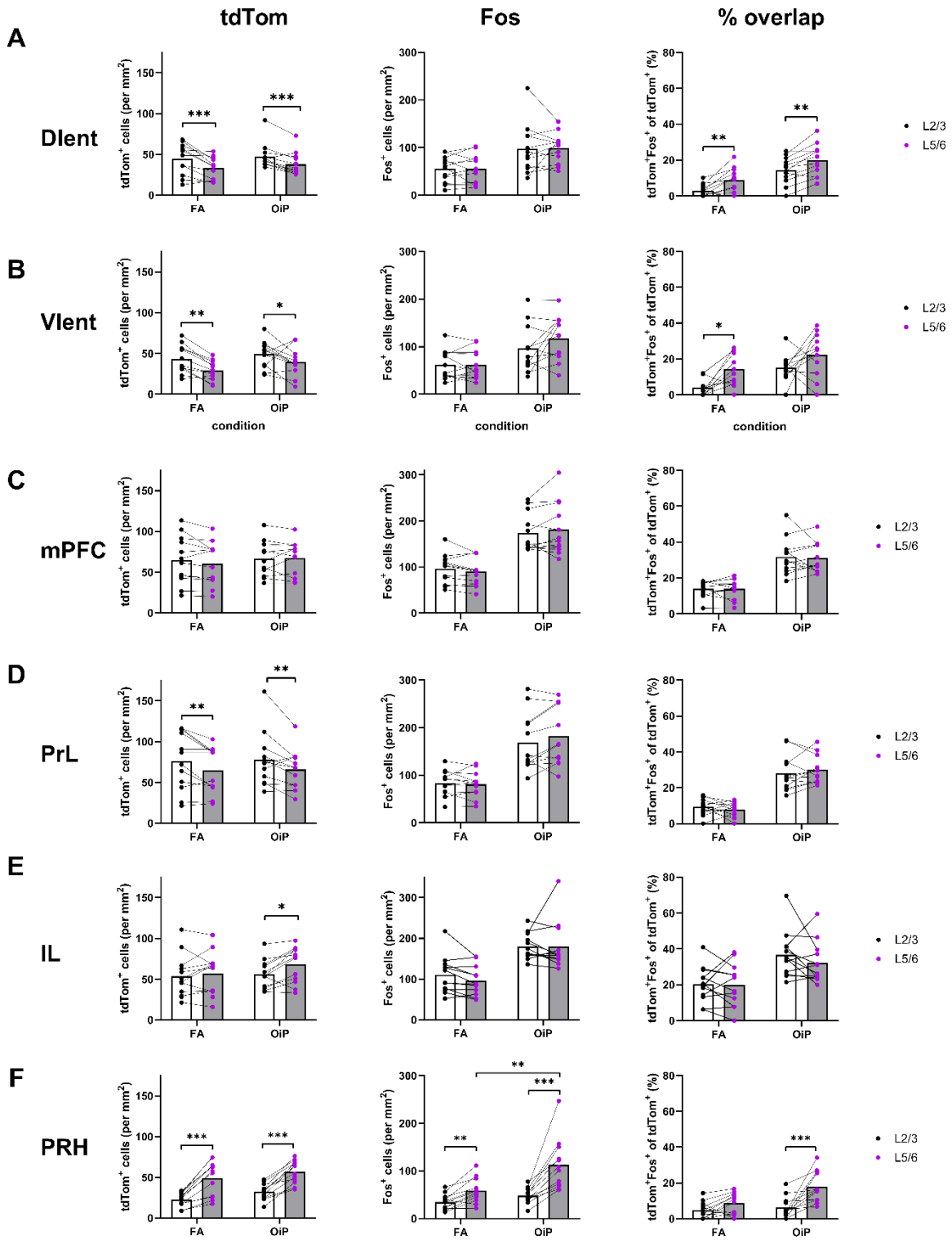

Supplementary Figure 2. Expression patterns of tdTom, Fos and overlap in layer 2/3 and layer 5/6 across cortical regions.

A: (Left to right) tdTom, Fos and percent overlap for L2/3 and L5/6 in DIent.

B: Same as A but for VIent.

C: Same as A but for mPFC.

D: Same as A but for PrL.

E: Same as A but for IL.

F: Same as A but for PRH

*** $p < 0.001$, ** $p < 0.01$, * $p < 0.05$. n = 12 mice per condition , bars represent mean values. See table S2 for detailed statistical analysis.

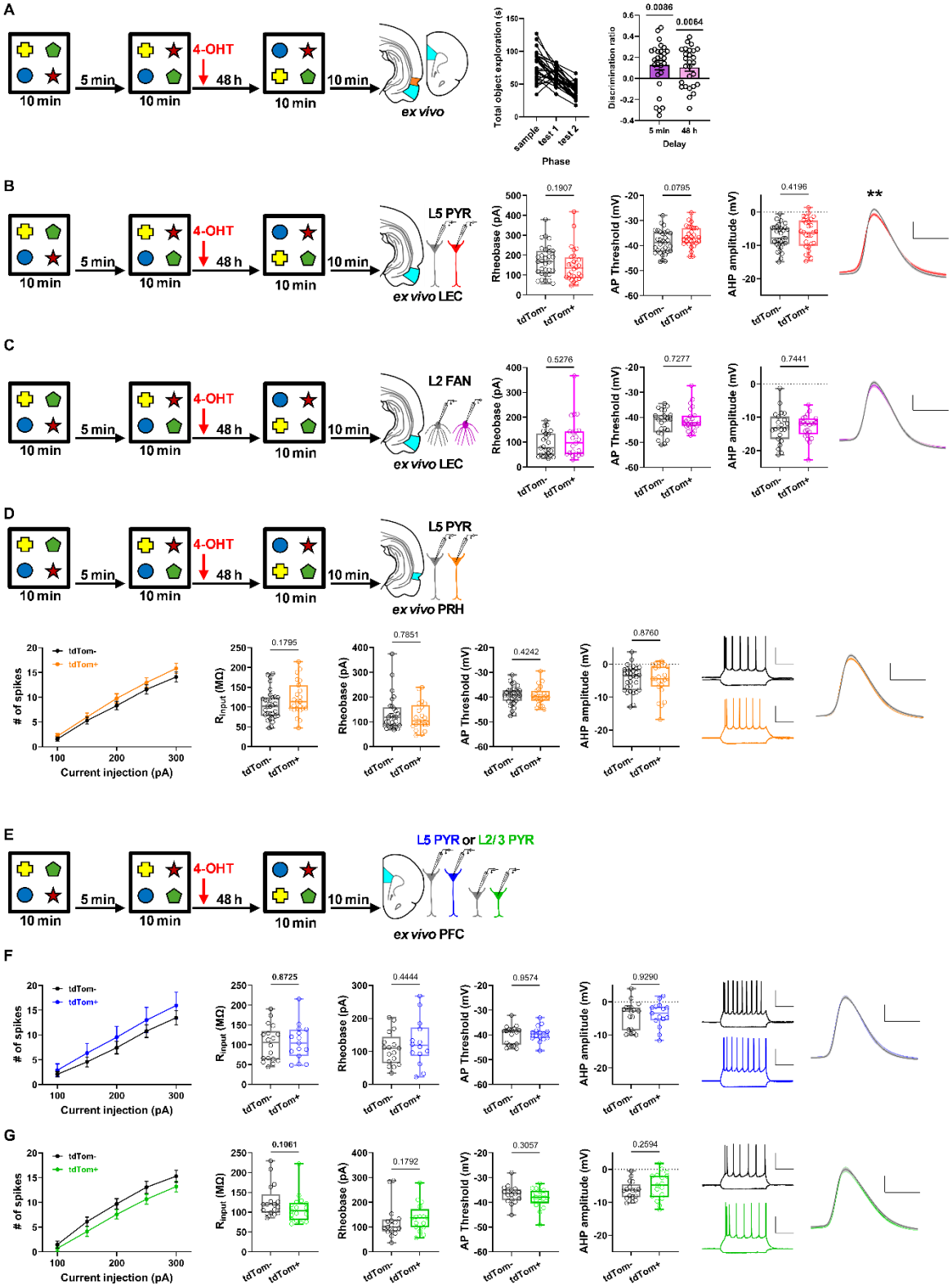

Supplementary Figure 3. Increased excitability following object reconfiguration is limited to LEC L5 pyramidal engram cells

A: (Left) Labelling strategy for *ex vivo* slice recordings from multiple brain regions from animals shown reconfigured objects before slicing. (Right) Total object exploration and discrimination ratios for animals shown reconfigured objects.

B: (Left) Labelling strategy for *ex vivo* L5 LEC pyramidal cell recordings from animals exposed to reconfigured objects before slicing. (Right) Further measures of cellular excitability related to Fig 3A, rheobase, action potential (AP) threshold, AHP amplitude and mean ± SEM AP waveforms for $tdTom^-$ and $tdTom^+$ cells.

C: Same as (B) but for L2 fan cells

D: (Top) Labelling strategy for *ex vivo* L5 perirhinal cortex (PRH) pyramidal cell recordings from animals exposed to reconfigured objects before slicing. (Bottom) Action potential firing, input resistance, rheobase, AP threshold, AHP amplitude, representative voltage responses and mean ± SEM AP waveforms of L5 PRH pyramidal cells.

E: Labelling strategy for *ex vivo* mPFC pyramidal cell recordings from animals exposed to reconfigured objects before slicing.

F: Action potential firing, input resistance, rheobase, AP threshold, AHP amplitude, representative voltage responses and mean ± SEM AP waveforms of L5 mPFC pyramidal cells.

G: Same as (F) but for L2/3 mPFC pyramidal cells.

Scale bars of representative voltage responses = 200 ms, 40 mV, AP waveforms = 1 ms, 20 mV.

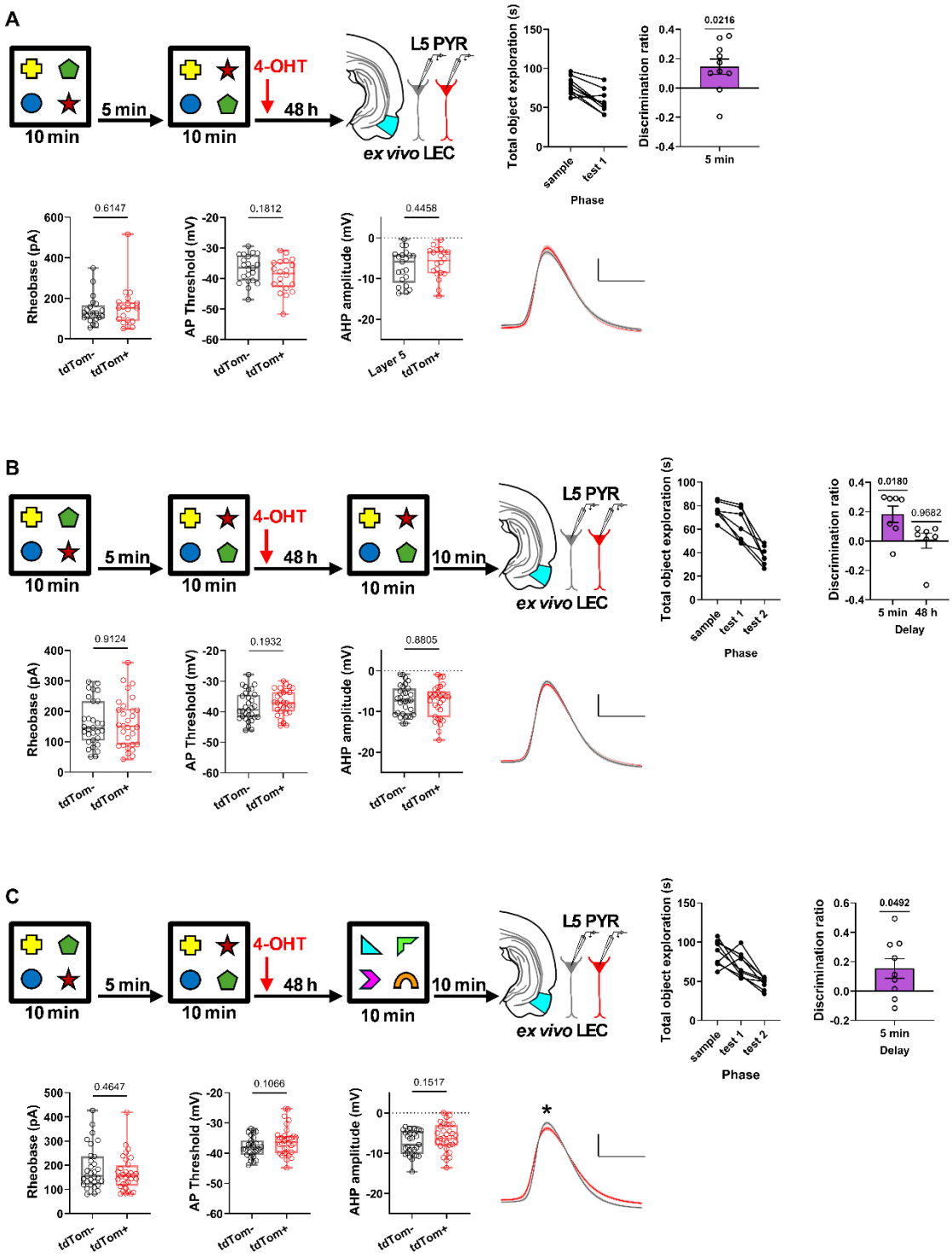

Supplementary Figure 4. Increased neuronal excitability of LEC L5 pyramidal neurons requires recall of engram specific cues with associated novel information

A: (Top row, left) Labelling strategy for *ex vivo* slices from animals which were not presented with a second test phase before slicing. (Top row, right) Total object exploration and discrimination ratios. (Bottom row) Rheobase, AP threshold, AHP amplitude and mean ± SEM AP waveforms of L5 PRH pyramidal cells. Data related to Fig 3C.

B: Same as (A) but for animals shown familiar object configuration. Data related to Fig 3D.

C: Same as (A) but for animals shown a novel object set before slicing. Data related to Fig 3E.

Scale bars = 1 ms, 20 mV.

Brain region	tdtom +ve cells	Fos +ve cells	% Overlap
mPFC	F(1,22)=0.17, p=0.686	F(1,22)=26.90, p=3.35 x 10^{-5}	F(1,22)=38.54, p=3.01 x10^{-6}
PrL	F(1,22)=0.01, p=0.909	F(1,22)=24.88, p=5.42 x 10^{-5}	F(1,22)=58.95, p=1.16 x10^{-7}
IL	F(1,22)=0.55, p=0.466	F(1,22)=21.20, p=1.38 x 10^{-4}	F(1,22)=11.78, p=0.002
LEC	F(1,22)=0.89, p=0.356	F(1,22)=10.325, p=0.004	F(1,22)=37.42, p=3.71 x 10^{-6}
DLent	F(1,22)=0.40, p=0.534	F(1,22)=9.40, p=0.006	F(1,22)=26.26, p=3.90 x10^{-5}
DIent	F(1,22)=0.39, p=0.537	F(1,22)=9.83, p=0.005	F(1,22)=20.59, p=1.62 x10^{-4}
VIent	F(1,22)=2.01, p=0.171	F(1,22)=9.33, p=0.006	F(1,22)=27.62, p=2.85 x 10^{-5}
PRH	F(1,22)=2.60, p=0.121	F(1,22)=9.26, p=0.006	F(1,22)=7.64, p=0.011

Supplementary table 1: Statistical analysis of tdTom and Fos expression and % overlap across mPFC & LEC and their subdivisions. Data shows outcome of one-way ANOVA with behavioural task as a between subjects factor. For both FA & OiP conditions n = 12.

Brain region	tdTom +ve cells	Fos +ve cells	% overlap
PFC	Depth by beh. cond. F(1,22)=1.43, p=0.244 Depth F(1,22)=1.28, p=0.270 Beh cond. F(1,22)=0.17, p=0.686	Depth by beh. cond. F(1,22)=3.03, p=0.096 Depth F(1,22)= 0.02, p=0.877 Beh cond. F(1,22)=26.90, p=3.4 x10^{-5}	Depth by beh. cond. F(1,22)=0.07, p=0.790 Depth F(1,22)=0.09, p=0.770 Beh cond. F(1,22)=39.22, p=3.0 x 10^{-6}
PrL	Depth by beh. cond. F(1,22)= 0.01, p=0.929 Depth F(1,22)= 13.70, p=0.001 Beh cond. F(1,22)= 0.01, p=0.909	Depth by beh. cond. F(1,22)=1.85, p=0.188 Depth F(1,22)=3.79, p=0.064 Beh cond. F(1,22)=24.88, p=5.42 x10^{-5}	Depth by beh. cond. F(1,22)=1.76, p=0.198 Depth F(1,22)=0.30, p=0.864 Beh cond. F(1,22)=61.68, p=8.01 x10^{-8}
IL	Depth by beh. cond. F(1,22)= 2.85, p=0.106 Depth F(1,22)= 7.99, p=0.010 Beh cond. F(1,22)= 0.55, p=0.466	Depth by beh. cond. F(1,22)=1.17, p=0.291 Depth F(1,22)=0.96, p=0.338 Beh cond. F(1,22)=21.20, p= 1.38 x10^{-4}	Depth by beh. cond. F(1,22)=0.76, p=0.394 Depth F(1,22)=1.09, p=0.308 Beh cond. F(1,22)=11.97, p=0.002
LEC	Depth by beh. cond. F(1,22)= 1.36, p=0.256 Depth F(1,22)=49.40, p=4.72 x 10^{-7} Beh cond. F(1,22)=0.89, p=0.356	Depth by beh. cond. F(1,22)=0.86, p=0.364 Depth F(1,22)=0.14, p=0.712 Beh cond. F(1,22)=10.33, p=0.004	Depth by beh. cond. F(1,22)=0.01, p=0.928 Depth F(1,22)=50.08, p=4.25 x 10^{-7} Beh cond. F(1,22)=32.75, p=9.34 x 10^{-6}
DLent	Depth by beh. cond. F(1,22)=0.27, p=0.606 Depth F(1,22)= 5.59, p=0.027 Beh cond. F(1,22)=0.40, p=0.534	Depth by beh. cond. F(1,22)= 0.04, p=0.847 Depth F(1,22)=1.52, p=0.231 Beh cond. F(1,22)=9.40, p=0.006	Depth by beh. cond. F(1,22)=0.03, p=0.870 Depth F(1,22)=26.18, p=4.04 x 10^{-5} Beh cond. F(1,22)=22.97, p=8.71 x 10^{-5}
DIent	Depth by beh. cond. F(1,22)=0.39, p=0.539 Depth F(1,22)=33.08, p=8.72x10^{-6} Beh cond. F(1,22)=0.39, p=0.537	Depth by beh. cond. F(1,22)=0.04, p=0.853 Depth F(1,22)=0.05, p=0.819 Beh cond. F(1,22)=9.83 p=0.005	Depth by beh. cond. F(1,22)=0.005, p=0.945 Depth F(1,22)=34.18, p=7.00 x 10^{-6} Beh cond. F(1,22)=18.21, p=3.14 x 10^{-4}
VIent	Depth by beh. cond. F(1,22)=0.55, p=0.467 Depth F(1,22)=15.96, p=6.11 x 10^{-4} Beh cond. F(1,22)=2.01, p=0.171	Depth by beh. cond. F(1,22)=2.55, p=0.125 Depth F(1,22)=2.55, p=0.125 Beh cond. F(1,22)=9.33 p=0.006	Depth by beh. cond. F(1,22)=0.31, p=0.583 Depth F(1,22)=11.25, p=0.003 Beh cond. F(1,22)=16.81, p=4.72 x 10^{-4}
PRH	Depth by beh. cond. F(1,22)=0.14, p=0.717 Depth F(1,22)=99.59, p=1.25x10^{-9} Beh cond. F(1,22)=2.60, p=0.121	Depth by beh. cond. F(1,22)=8.66, p=0.008 Depth F(1,22)=40.84, p=1.98x10^{-6} Beh cond. F(1,22)=9.26, p=0.006	Depth by beh. cond. F(1,22)=5.56, p=0.028 Depth F(1,22)=21.03, p=1.44x10^{-4} Beh cond. F(1,22)=6.94, p=0.015

Supplementary table 2: Statistical analysis of tdTom and Fos expression and % overlap in superficial and deep layers of prefrontal and lateral entorhinal cortex. Data shows outcome of two-way ANOVA with behavioural condition (beh. cond.) as a between-subjects factor and depth as a within-subjects factor. For both FA and OiP condition n = 12.

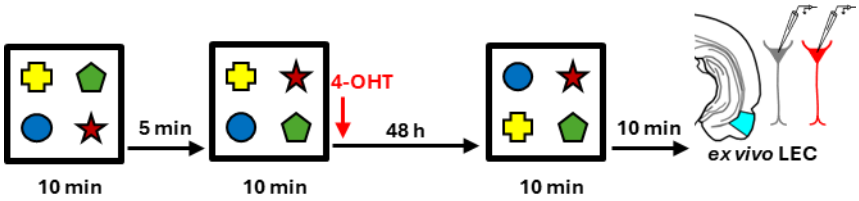

Physiological property	tdTom- L5 LEC pyramidal cells (n = 31 cells from 16 mice)	tdTom+ L5 LEC pyramidal cells (n = 28 cells from 16 mice)	Mann Whitney U	P-value
Resting membrane potential (mV)	-64.90 (-67.00, -62.00)	-64.20 (-66.40, -61.33)	379	0.409
Input resistance (MΩ)	74.93 (63.80, 108.9)	108.7 (76.33,141.7)	261	**0.0081**
Tau (ms)	20.34 (14.28, 25.48)	19.12 (15.62, 22.42)	376	0.386
Sag (%)	13.25 (5.33, 22.11)	14.61 (6.12, 18.68)	418	0.815
Rheobase (pA)	167.3 (107.1, 221.0)	135.3 (85.16, 188.0)	347	0.191
Action potential threshold (mV)	-38.86 (-42.38, -34.86)	-37.01 (-39.17, -33.07)	318	0.0795
Afterhyperpolarisation (mV)	-7.84 (-9.65, -4.73)	-6.07 (-10.11, -2.55)	380	0.420
Medium afterhyperpolarisation amplitude (mV)	-2.60 (-3.71, -1.01)	-1.81 (-2.94, -1.01)	374	0.369
Medium afterhyperpolarisation area (mV.ms)	-0.20 (-0.28, -0.07)	-0.14 (-0.23, -0.07)	377	0.394
ADP presence (# cells)	14/31	11/28	$\chi^2 = 0.21$	0.648
ADP amplitude (mV)	0.18 (0.10, 0.86)*	0.31 (0.17, 1.46)	42	0.093
Action potential amplitude (mV)	74.83 (70.02, 82.44)	66.09 (58.63, 77.42)	247	**0.0041**
AP half width (ms)	0.81 (0.74, 0.95)	0.84 (0.77, 0.98)	361	0.273
AP max rate of rise ($mV.ms^{-1}$)	326.7 (262.5, 413.6)	248.8 (208.0, 349.9)	271	**0.013**
Cells in DLE	22	18		
Cells in DIE	9	9		
Cells in VIE	0	1		
Cell firing	**Mixed-effects model**	**Factor**	**F**	**P-value**
		Current	$F_{(1.4, 80)} = 268.1$	**$<1x10^{-15}$**
		Labelling	$F_{(1, 57)} = 4.92$	**0.031**
		Interaction	$F_{(4,228)} = 3.72$	**0.006**

Supplementary table 3. Summary of physiological properties of layer 5 LEC tdTom- and tdTom+ pyramidal neurons recorded from ex vivo slices from animals which underwent a second test phase (related to Fig 3A). Values represent median (25, 75 percentiles). Reported statistical values show Mann Whitney U test with 2-tailed p-value, except for ADP presence which uses Chi-squared test with 2-tailed p value. *one value was excluded from analysis due to spiking during ADP.

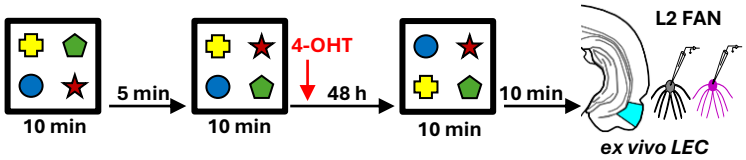

Physiological property	tdTom- L2a fan cells (n = 23 cells from 16 mice)	tdTom+ L2a fan cells pyramidal cells (n = 23 cells from 17 mice)	Mann Whitney U	P-value
Resting membrane potential (mV)	-63.80 (-67.60, -62.10)	-63.40 (-66.20, -58.50)	205.5	0.199
Input resistance (MΩ)	198.2 (129.0, 247.6)	156.9 (108.7, 219.2)	210	0.238
Tau (ms)	21.05 (16.74, 25.03)	21.24 (15.03, 27.28)	255	0.845
Sag (%)	15.34 (8.71, 19.38)	13.40 (7.17, 20.52)	241	0.617
Rheobase (pA)	75.93 (47.28, 133.8)	95.70 (52.09, 144.0)	235	0.528
Action potential threshold (mV)	-40.82 (-46.07, -39.18)	-42.13 (-43.49, -39.39)	248	0.728
Afterhyperpolarisation (mV)	-13.22 (-16.49, -9.86)	-11.95 (-15.13, -10.36)	249	0.744
Medium afterhyperpolarisation amplitude (mV)	-1.54 (-1.97, -0.73)	-1.28 (-1.74, -0.31)	212	0.256
Medium afterhyperpolarisation area (mV.ms)	-0.13 (-0.15, -0.05)	-0.10 (-0.13, -0.02)	208	0.221
ADP presence (# cells)	6/17	9/14	$\chi^2 = 0.89$	0.345
ADP amplitude (mV)	0.33 (0.07, 0.66)	0.15 (0.07, 0.45)	26	0.955
Action potential amplitude (mV)	81.03 (69.03, 84.64)	78.32 (58.48, 85.04)	217	0.305
AP half width (ms)	0.80 (0.75, 0.97)	0.82 (0.75, 0.95)	250	0.761
AP max rate of rise ($mV.ms^{-1}$)	343.5 (265.6, 375.0)	309.6 (210.0, 378.7)	232.5	0.489
Cells in DLE	10	12		
Cells in DIE	11	10		
Cells in VIE	2	1		
Cell firing	**Mixed-effects model**	**Factor**	**F**	**P-value**
		Current	$F_{(2.0, 85.5)} = 384$	**$<1x10^{-15}$**
		Labelling	$F_{(1,44)} = 1.00$	0. 32
		Interaction	$F_{(4,174)} = 0.77$	0.55

Supplementary table 4. Summary of physiological properties of layer 2a LEC tdTom- and tdTom+ fan cells recorded from ex vivo slices from animals which underwent a second test phase (related to Fig 3B, S3B). Values represent median (25th, 75th percentiles). Reported statistical values show Mann Whitney U test with 2-tailed p-value, except for ADP presence which uses Chi-squared test with 2-tailed p value.

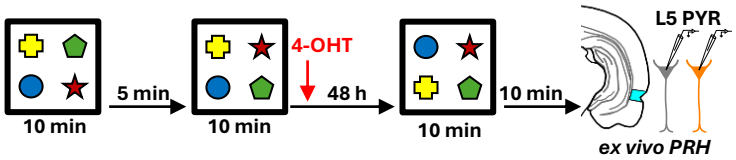

Physiological property	tdTom- L5 PRH pyramidal cells (n = 31 cells from 14 mice)	tdTom+ L5 PRH pyramidal cells (n = 23 cells from 13 mice)	Mann Whitney U	P-value
Resting membrane potential (mV)	-63.80 (-66.30, -60.80)	-64.00 (-66.30, -61.20)	330.5	0.655
Input resistance (MΩ)	102 (77.98, 124.6)	113.2 (95.74, 155.4)	279	0.180
Tau (ms)	17.76 (15.02, 22.09)	18.00 (14.10, 23.43)	351	0.931
Sag (%)	15.35 (9.49, 19.15)	13.99 (10.15, 20.21)	355	0.986
Rheobase (pA)	117.4 (84.16, 158.2)*	104.7 (86.00, 166.8)*	290	0.785
Action potential threshold (mV)	-39.15 (-41.63, -37.34)	-39.78 (-41.54, -37.44)	310	0.424
Afterhyperpolarisation (mV)	-3.48 (-7.83, -1.50)	-4.44 (-6.78, -0.77)	347	0.876
Medium afterhyperpolarisation amplitude (mV)	-2.57 (-3.61, -1.20)	-2.48 (-3.33, -1.32)	355	0.986
Medium afterhyperpolarisation area (mV.ms)	-0.19 (-0.29, -0.07)	-0.17 (-0.27, -0.09)	352	0.945
ADP presence (# cells)	12/31	11/23	$\chi^2 = 0.45$	0.503
ADP amplitude (mV)	0.31 (0.09, 0.71)	0.13 (0.05, 0.89)	58	0.651
Action potential amplitude (mV)	71.49 (65.10, 79.21)	66.82 (63.67, 71.70)	251	0.066
AP half width (ms)	0.89 (0.81, 1.05)	0.92 (0.83, 1.02)	327	0.615
AP max rate of rise ($mV.ms^{-1}$)	272.5 (212.4, 343.5)	256.3 (211.2, 286.4)	270	0.133
Cell firing	**Mixed-effects model**	**Factor**	**F**	**P-value**
		Current	$F_{(1.5, 74.9)} = 415$	**$<1x10^{-15}$**
		Labelling	$F_{(1,52)} = 1.04$	0.31
		Interaction	$F_{(4,207)} = 0.87$	0.48

Supplementary table 5. Summary of physiological properties of layer 5 perirhinal cortex tdTom- and tdTom+ neurons recorded from ex vivo slices from animals which underwent a second test phase (related to Fig S3D). Values represent median (25, 75 percentiles). Reported statistical values show Mann Whitney U test with 2-tailed p-value, except for ADP presence which uses Chi-squared test with 2-tailed p value. **data not collected for 2 cells*.

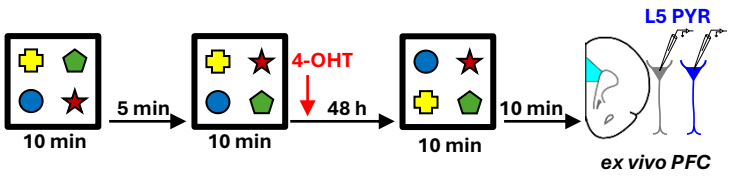

Physiological property	tdTom- L5 mPFC pyramidal cells (n = 18 cells from 5 mice)	tdTom+ L5 mPFC pyramidal cells (n = 15 cells from 5 mice)	Mann Whitney U	P-value
Resting membrane potential (mV)	-64.20 (-66.15, -63.10)	-64.90 (-67.40, -61.80)	127	0.782
Input resistance (MΩ)	105.5 (62.78, 133.9)	104.6 (72.01, 138.8)	130	0.873
Tau (ms)	13.35 (9.43, 18.43)	13.76 (9.08, 15.20)	133	0.957
Sag (%)	7.89 (5.11, 11.34)	4.38 (2.31, 13.33)	110	0.381
Rheobase (pA)	109.5 (64.41, 143.5)*	117.7 (85.06, 171.9)*	99	0.444
Action potential threshold (mV)	-38.68 (-44.07, -37.74)	-39.63 (-41.18, -38.33)	133	0.957
Afterhyperpolarisation (mV)	-2.84 (-8.63, -1.70)	-3.45 (-5.59, -1.40)	132	0.929
Medium afterhyperpolarisation amplitude (mV)	-2.05 (-2.70, -1.06)**	-1.11 (-3.11, -0.48)***	83	0.720
Medium afterhyperpolarisation area (mV.ms)	-0.15 (-0.18, -0.07)**	-0.08 (-0.19, -0.03)***	80	0.616
ADP presence (# cells)	8/18	9/15	$\chi^2 = 0.79$	0.373
ADP amplitude (mV)	0.94 (0.32, 1.70)	0.79 (0.12, 1.56)	39.50	0.677
Action potential amplitude (mV)	67.87 (64.00, 79.48)	68.92 (65.45, 76.16)	134	0.986
AP half width (ms)	0.88 (0.80, 0.98)	0.92 (0.75, 1.01)	123	0.682
AP max rate of rise ($mV.ms^{-1}$)	271.4 (244.4, 348.9)	266.4 (236.3, 322.8)	131	0.901
Cell firing	**Mixed-effects model**	**Factor**	**F**	**P-value**
		Current	$F_{(1.2, 37.7)} = 144$	**$<1x10^{-15}$**
		Labelling	$F_{(1,31)} = 0.68$	0.41
		Interaction	$F_{(4,123)} = 0.58$	0.68

Supplementary table 6. Summary of physiological properties of layer 5 medial prefrontal cortex tdTom- and tdTom+ neurons recorded from ex vivo slices from animals which underwent a second test phase (related to Fig S3E-F). Values represent median (25, 75 percentiles). Reported statistical values show Mann Whitney U test with 2-tailed p-value, except for ADP presence which uses Chi-squared test with 2-tailed p value. **data not collected for 1 cells. ** data not collected for 4 cells. ***data not collected for 3 cells.*

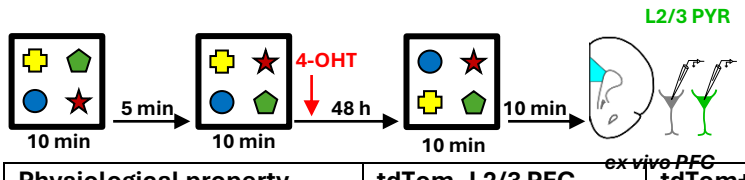

Physiological property	tdTom- L2/3 PFC pyramidal cells (n = 17 cells from 5 mice)	tdTom+ L2/3 PFC pyramidal cells (n = 17 cells from 5 mice)	Mann Whitney U	P-value
Resting membrane potential (mV)	-64.30 (-66.05, -62.25)	-63.40 (-66.20, -60.85)	133	0.702
Input resistance (MΩ)	119.7 (98.06, 145.4)	103.4 (80.49, 123.5)	97	0.106
Tau (ms)	16.04 (12.81, 17.89)	14.99 (12.39, 19.34)	139	0.865
Sag (%)	3.53 (-2.67, 7.63)	2.28 (-2.63, 4.07)	122	0.454
Rheobase (pA)	99.36 (82.68, 130.0)	137.6 (99.35, 172.7)*	98	0.179
Action potential threshold (mV)	-36.58 (-39.02, -34.76)	-37.94 (-40.38, -35.39)	114	0.306
Afterhyperpolarisation (mV)	-6.38 (-8.50, -4.53)	-4.81 (-8.48, -1.91)	111	0.260
Medium afterhyperpolarisation amplitude (mV)	-0.81 (-2.04, -0.36)	-1.13 (-2.32, -0.34)*	131	0.873
Medium afterhyperpolarisation area (mV.ms)	-0.06 (-0.15, -0.02)	-0.09 (-0.19, -0.02)*	131	0.873
ADP presence (# cells)	10/17	7/17	χ^2 = 1.06	0.303
ADP amplitude (mV)	0.32 (1.13, 1.03)	0.22 (0.04, 1.02)	19	0.535
Action potential amplitude (mV)	65.22 (57.95, 78.93)	69.56 (62.72, 76.75)	131	0.658
AP half width (ms)	0.99 (0.91, 1.07)	0.93 (0.85, 1.00)	114	0.306
AP max rate of rise (mV.ms^{-1})	237.5 (209.4, 337.8)	268.6 (235.0, 343.9)	117	0.357
Cell firing	**Mixed-effects model**	**Factor**	**F**	**P-value**
		Current	$F_{(1.5, 46.4)}$ = 424	**<1x10^{-15}**
		Labelling	$F_{(1,32)}$ = 2.04	0.16
		Interaction	$F_{(4,127)}$ = 1.6	0.18

Supplementary table 7. Summary of physiological properties of layer 2/3 prefrontal cortex tdTom- and tdTom+ neurons recorded from ex vivo slices from animals which underwent a second test phase (related to Fig S3E, S3G). Values represent median (25, 75 percentiles). Reported statistical values show Mann Whitney U test with 2-tailed p-value, except for ADP presence which uses Chi-squared test with 2-tailed p value. **data not collected for 1 cell*.

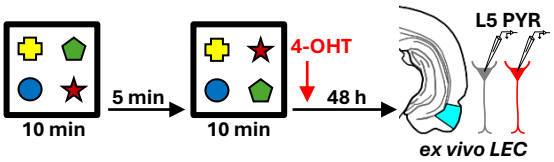

Physiological property	tdTom- L5 LEC pyramidal cells (n = 21 cells from 10 mice)	tdTom+ L5 LEC pyramidal cells (n = 20 cells from 10 mice)	Mann Whitney U	P-value
Resting membrane potential (mV)	-62.80 (-64.95,-59.50)	-62.30 (-63.63, -57.95)	173.5	0.348
Input resistance (MΩ)	82.62 (68.61, 127.0)	71.69 (53.29, 111.6)	172	0.332
Tau (ms)	15.82 (12.94, 21.21)	16.17 (13.64, 19.36)	209	0.990
Sag (%)	12.63 (6.05, 15.85)	10.94 (2.69, 24.55)	201	0.826
Rheobase (pA)	126.7 (101.5, 165.5)	152.7 (88.09, 181.8)	190	0.615
Action potential threshold (mV)	-36.52 (-40.73,-32.45)	-38.37 (-42.89, -34.63)	158	0.181
Afterhyperpolarisation (mV)	-5.88 (-11.02, -4.13)	-5.58 (-8.76, -3.25)	180	0.446
Medium afterhyperpolarisation amplitude (mV)	-1.80 (-2.93, -0.56)	-1.45 (-3.13, -0.52)	207	0.949
Medium afterhyperpolarisation area (mV.ms)	-0.131 (-0.227,-0.030)	-0.114 (-0.236, -0.025)	203	0.867
ADP presence (# cells)	4/21	5/20	$\chi^2 = 0.21$	0.645
ADP amplitude (mV)	0.597 (0.112, 2.25)	0.348 (0.157, 1.45)	8	0.730
Action potential amplitude (mV)	63.27 (59.73, 69.17)	73.25 (62.63, 80.74)	146	0.098
AP half width (ms)	0.916 (0.772, 0.966)	0.837 (0.791, 0.939)	195	0.703
AP max rate of rise ($mV.ms^{-1}$)	241.0 (212.2, 321.7)	294.3 (251.8, 380.6)	148	0.109
Cells in DLE	19	18		
Cells in DIE	1	1		
Cells in VIE	1	1		
Cell firing	**Mixed-effects model**	**Factor**	**F**	**P-value**
		Current	$F_{(1.6, 60.35)} = 153$	**$<1x10^{-15}$**
		Labelling	$F_{(1,39)} = 0.003$	0.96
		Interaction	$F_{(4,156)} = 0.55$	0.76

Supplementary table 8. Summary of physiological properties of layer 5 LEC tdTom- and tdTom+ neurons recorded from ex vivo slices from animals which did not undergo a second test phase (related to Fig 3C, S4A). Values represent median (25, 75 percentiles). Reported statistical values show Mann Whitney U test with 2-tailed p-value, except for ADP presence which uses Chi-squared test with 2-tailed p value.

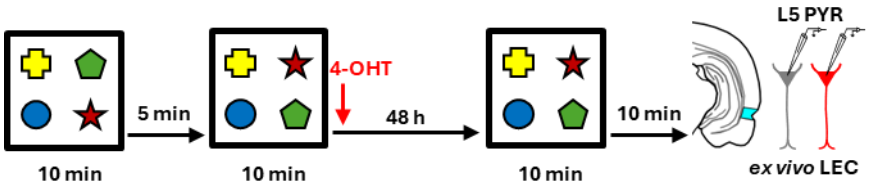

Physiological property	tdTom- L5 LEC pyramidal cells (n = 31 cells from 7 mice)	tdTom+ L5 LEC pyramidal cells (n = 30 cells from 7 mice)	Mann Whitney U	P-value
Resting membrane potential (mV)	-65.30 (-67.90, -62.10)	-64.30 (-66.80, -62.73)	425.5	0.574
Input resistance (MΩ)	76.07 (56.03, 102.3)	81.98 (56.31, 99.60)	449	0.824
Tau (ms)	17.01 (13.61, 19.64)	15.12 (12.16, 19.56)	434	0.662
Sag (%)	11.73 (6.02, 16.94)	10.28 (5.48, 16.78)	454	0.881
Rheobase (pA)	144.2 (103.6, 233.5)*	150.3 (90.40, 207.8)	442	0.912
Action potential threshold (mV)	-39.42 (-41.80, -34.39)	-37.13 (-39.89, -33.55)	374	0.193
Afterhyperpolarisation (mV)	-7.32 (-10.78, -4.34)	-6.53 (-11.40, -5.10)	454	0.881
Medium afterhyperpolarisation amplitude (mV)	-1.42 (-2.24, -0.84)*	-1.81 (-2.95, -0.75)*	389	0.493
Medium afterhyperpolarisation area (mV.ms)	-0.11 (-0.17, -0.06)*	-0.12 (-0.23, -0.05)*	384	0.447
ADP presence (# cells)	4/30*	8/22	$\chi^2 = 1.67$	0.197
ADP amplitude (mV)	0.12 (0.09, 1.58)*	1.46 (0.45, 1.86)	10	0.368
Action potential amplitude (mV)	72.01 (63.73, 79.43)	67.06 (60.68, 78.51)	369	0.170
AP half width (ms)	0.81 (0.78, 0.91)	0.84 (0.75, 0.90)	438	0.704
AP max rate of rise ($mV.ms^{-1}$)	303.7 (262.5, 377.0)	269.3 (226.4, 362.3)	388	0.272
Cells in DLE	29	28		
Cells in DIE	2	2		
Cells in VIE	0	0		
Cell firing	**Mixed-effects model**	**Factor**	**F**	**P-value**
		Current	$F_{(1.3, 74.68)} = 156$	**$<1x10^{-15}$**
		Labelling	$F_{(1,59)} = 0.004$	0.85
		Interaction	$F_{(4,236)} = 0.34$	0.86

Supplementary table 9. Summary of physiological properties of layer 5 LEC tdTom- and tdTom+ neurons recorded from ex vivo slices from animals exposed to familiar object configuration at test 2 (related to Fig 3D, S4B). Values represent median (25, 75 percentiles). Reported statistical values show Mann Whitney U test with 2-tailed p-value, except for ADP presence which uses Chi-squared test with 2-tailed p value. * data not collected for one cell for indicated data set.

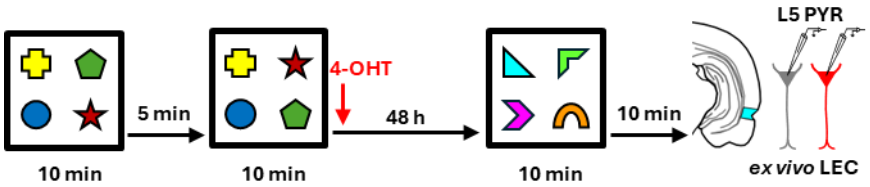

Physiological property	tdTom- L5 LEC pyramidal cells (n = 31 cells from 9 mice)	tdTom+ L5 LEC pyramidal cells (n = 32 cells from 9 mice)	Mann Whitney U	P-value
Resting membrane potential (mV)	-63.20 (-64.90, -61.00)	-63.20 (-67.20, -58.05)	249.5	0.997
Input resistance (MΩ)	81.63 (62.60, 102.8)	88.21 (57.89, 125.2)	445	0.490
Tau (ms)	16.24 (12.68, 18.26)	16.14 (13.78, 18.04)	473	0.759
Sag (%)	14.55 (7.05, 21.85)	11.86 (5.67, 17.77)	396	0.173
Rheobase (pA)	155.5 (120.1, 236.8)	156.3 (115.2, 199.4)	442	0.465
Action potential threshold (mV)	-38.03 (-40.52, -35.82)	-36.35 (-39.92, -34.28)	378	0.107
Afterhyperpolarisation (mV)	-7.86 (-10.15, -4.48)	-6.27 (-8.13, -3.06)	391	0.152
Medium afterhyperpolarisation amplitude (mV)	-2.26 (-3.73, -1.34)	-1.50 (-2.75, -0.83)	378	0.107
Medium afterhyperpolarisation area (mV.ms)	-0.16 (-0.27, -0.10)	-0.12 (-0.21, -0.06)	389	0.144
ADP presence (# cells)	16/31	9/32	$\chi^2 = 1.91$	0.057
ADP amplitude (mV)	0.48 (0.17, 0.88)	0.38 (0.24, 1.38)	71	0.978
Action potential amplitude (mV)	71.33 (63.40, 78.38)	64.15 (55.35, 73.36)	337	**0.029**
AP half width (ms)	0.79 (0.72, 0.87)	0.88 (0.79, 0.94)	289	**0.004**
AP max rate of rise ($mV.ms^{-1}$)	293.0 (240.2, 373.0)	241.8 (199.6, 302.3)	298.5	**0.006**
Cells in DLE	29	29		
Cells in DIE	2	3		
Cells in VIE	0			
Cell firing	**Mixed-effects model**	**Factor**	**F**	**P-value**
		Current	$F_{(1.3, 81.67)} = 182$	**$<1x10^{-15}$**
		Labelling	$F_{(1,61)} = 0.001$	0.97
		Interaction	$F_{(4,244)} = 0.23$	0.92

Supplementary table 10. Summary of physiological properties of layer 5 LEC tdTom- and tdTom+ neurons recorded from ex vivo slices from animals were exposed to a new object set prior to slice preparation (related to Fig 3E, S4C). Values represent median (25, 75 percentiles). Reported statistical values show Mann Whitney U test with 2-tailed p-value, except for ADP presence which uses Chi-squared test with 2-tailed p value.

Section	AP position, relative to bregma	Brain regions analysed
mPFC 1	+2.33mm to +1.97mm	PrL
mPFC 2	+1.97mm to +1.77mm	PrL, IL
mPFC 3	+1.77mm to +1.41mm	PrL, IL
mPFC 4	+1.41mm to +1.33mm	IL
LEC 1	-2.91mm to -3.15mm	PRH, DLent, DIent
LEC 2	-3.15mm to -3.27mm	PRH, DLent, DIent
LEC 3	-3.39mm to -3.63mm	PRH, DLent, DIent, Vient
LEC 4	-3.79mm to -4.10mm	PRH, DLent, DIent, Vient
LEC 5	-4.23mm to -4.47mm	PRH, DLent, DIent, VIent

Supplementary table 11: Anterior-posterior position relative to bregma of coronal sections analysed for tdTom and Fos expression and overlap. PrL: prelimbic cortex, IL: infralimbic cortex, PRH: perirhinal cortex, DLent: dorsal lateral entorhinal cortex, DIent: dorsal intermediate entorhinal cortex, Vient: ventral intermediate entorhinal cortex.